PRELIMINARY ANALYSIS OF THE QUEEN CREEK, ARIZONA (QCAZ) STRAIN SYSTEM INCLUDING COMPARISON WITH THE TFO LONG-PERIOD ARRAY

14 April 1969

Prepared For

AIR FORCE TECHNICAL APPLICATIONS CENTER
Washington, D. C.

By

J. R. Woolson

SEISMIC DATA LABORATORY

Under

Project VELA UNIFORM

Sponsored By

ADVANCED RESEARCH PROJECTS AGENCY
Nuclear Monitoring Research Office
ARPA Order No. 624

PRELIMINARY ANALYSIS OF THE QUEEN CREEK, ARIZONA (QCAZ) STRAIN SYSTEM INCLUDING COMPARISON WITH THE TFO LONG-PERIOD ARRAY

SEISMIC DATA LABORATORY REPORT No. 271

AFTAC Project No.:	VELA T/0706
Project Title:	Seismic Data Laboratory
ARPA Order No.:	624
ARPA Program Code No.:	9F10
Name of Contractor:	TELEDYNE GEOTECH
Contract No.:	F33657-70-C-0941
Date of Contract:	01 April 1970
Amount of Contract:	$ 1,828,736
Contract Expiration Date:	30 June 1971
Project Manager:	Royal A. Hartenberger (703) 836-7647

P. O. Box 334, Alexandria, Virginia

APPROVED FOR PUBLIC RELEASE; DISTRIBUTION UNLIMITED.

DOCUMENT CONTROL DATA · R&D
(Security classification of title, body of abstract and indexing annotation must be entered when the overall report is classified)

1. ORIGINATING ACTIVITY (Corporate author)	2a. REPORT SECURITY CLASSIFICATION
TELEDYNE GEOTECH	Unclassified
ALEXANDRIA, VIRGINIA	2b. GROUP

3. REPORT TITLE

PRELIMINARY ANALYSIS OF THE QUEEN CREEK, ARIZONA (QCAZ) STRAIN SYSTEM INCLUDING COMPARISON WITH THE TFO LONG-PERIOD ARRAY

4. DESCRIPTIVE NOTES (Type of report and inclusive dates)

Scientific

5. AUTHOR(S) (Last name, first name, initial)

Woolson, J.R.

6. REPORT DATE	7a. TOTAL NO. OF PAGES	7b. NO. OF REFS
14 April 1971	56	8

8a. CONTRACT OR GRANT NO.	9a. ORIGINATOR'S REPORT NUMBER(S)
F33657-70-C-0941	271
b. PROJECT NO. VELA T/0706	
ARPA Order No. 624	9b. OTHER REPORT NO(S) (Any other numbers that may be assigned this report)
ARPA Program Code No. 9F10	

10.

APPROVED FOR PUBLIC RELEASE; DISTRIBUTION UNLIMITED.

11. SUPPLEMENTARY NOTES	12. SPONSORING MILITARY ACTIVITY
	ADVANCED RESEARCH PROJECTS AGENCY NUCLEAR MONITORING RESEARCH OFFICE WASHINGTON, D. C.

13. ABSTRACT

For seven earthquakes a comparison is made between the TFO long-period horizontal array and the sum of the horizontal strain and pendulum instruments at QCAZ. The performance of both systems was severely limited by noise of non-seismic origin. Within these limits the performance of the two systems is about equal. This report is preliminary in the sense that the installation of instruments at QCAZ was not complete at the time data were obtained. A lower level of non-seismic noise is to be expected when installation is complete.

Detailed analysis of one Chiapas, Mexico, earthquake demonstrates that strain-pendulum combinations can be used to enhance and identify both body and surface waves.

14. KEY WORDS

Strain System
Comparison
TFO Long Period Array

ABSTRACT

For seven earthquakes a comparison is made between the TFO long-period horizontal array and the sum of the horizontal strain and pendulum instruments at QCAZ. The performance of both systems was severely limited by noise of non-seismic origin.*Within these limits, the performance of the two systems is about equal. This report is preliminary in the sense that the installation of instruments at QCAZ was not complete at the time the data were obtained. A lower level of non-seismic noise is to be expected when installation is complete.

Detailed analysis of one Chiapas, Mexico, earthquake demonstrates that strain-pendulum combinations can be used to enhance and identify both body and surface waves.

*Detail comparison is made for one earthquake between QCAZ and the beamed vertical and horizontal array at TFO.

TABLE OF CONTENTS

LIST OF FIGURES

LIST OF FIGURES (Cont'd.)

INTRODUCTION AND THEORY

The new Queen Creek, Arizona, (QCAZ) strain seismograph system is about 125 km south of the Tonto Forest Observatory (TFO). Figure 1 is an index map of Arizona which shows the relation of QCAZ to the TFO long period array. The strain seismograph installation at QCAZ is described by Fix and Sherwin (1970).

Seven earthquakes were selected for analysis whose arrival azimuths at QCAZ would be near the installed azimuths of the horizontal strain seismographs, 55°(235°) and 325°(145°). Figure 2 is an equal azimuth world map centered at QCAZ on which are plotted the locations of the seven earthquakes used in this study. USC&GS data for these events are listed in Appendix I.

Benioff (1962) described the use of combinations of horizontal strain and pendulum seismometers to enhance body and surface waves. The response of a horizontal strain seismometer to longitudinal plane waves contains a factor $\cos^2\alpha$, where α is the angle between the strain rod and the direction of propagation of the wave. The response of a horizontal pendulum contains the factor $\cos \alpha$ (Benioff, 1935). Figure 3 shows the azimuthal response of a horizontal strain seismometer and a horizontal pendulum to longitudinal waves (or to the horizontal component of Rayleigh waves). When the outputs are summed, the combined response is as shown in Figure 4. To interpret this plot it is important to remember that the azimuth to an event is 180° opposite to its direction of propagation. In our applications both the sum and difference of the outputs have usually been calculated. For the 55° (northeast) azimuth pair the sum is a beam to the southwest and the difference (strain

-1-

minus pendulum) is a beam to the northeast. In order to sum the outputs, it is necessary that response of the instruments be matched. This is commonly accomplished in the recording process.

The response of the strain seismograph to transverse waves (SH or Love waves) is proportional to (sin α)·(cos α), where α is the angle between the direction of propagation of the earthquake and the installed azimuth of the strain rod (Benioff, 1935). Figure 5 shows the response of a horizontal strain seismograph to transverse waves. An orthogonal pair of strain seismographs can be used to enhance transverse waves, providing the direction of propagation is between about 30° to 60° from the installed azimuth: this is accomplished by computing the sum (to cancel) and difference (to enhance) of the wave.

Transverse phases whose direction of propagation is within 20° of the installed azimuth can be recognized by the fact that they are recorded by the transverse pendulum but not by either of the orthogonal strain instruments. Strain seismographs can not be rotated to produce radial and transverse components as are pendulum seismographs. The reason for this is that the transformation equation to a new coordinate system contains a shear component of strain which is not recorded by an orthogonal pair of instruments. A third strain seismograph at, e.g., 45° to the orthogonal pair can be used to record the shear component, providing that the usual plane strain assumptions are applicable (Jaeger, 1956).

In comparing the TFO long-period horizontal array to the QCAZ strain installation it was necessary to eliminate some elements from the TFO array. One instrument, at site 2, was inoperative during the period 19 to 25 May 1970, when the comparison was made, so this site has thus been eliminated from the computations. There also exists non-stationary, impulsive,

low-frequency (T ≃ 60 secs) noise on the horizontal long-period instruments, which was large enough to contaminate the comparison. Channels on which this noise occurred have in some cases been eliminated. A similar type of noise occurred on the 325° azimuth strain instrument at QCAZ. Commonly the effect of this noise was eliminated by filtering with a 15 to 50 second pass-band and by selecting samples which as far as possible did not include the noise. Examples of the noise described are marked with a dashed line block on several figures in the results section of this report.

Figures 6 and 7 are a comparison of the theoretical horizontal beam response pattern for TFO and QCAZ. A 235° azimuth beam has been chosen, corresponding to the 55° azimuth strain installation at QCAZ. This beam is toward the South Pacific region from which a number of earthquakes are recorded. In both cases for TFO a 20 second period, 3.0 km/sec wave has been chosen to determine the response. At QCAZ, it is assumed that the local phase velocity is constant with period, and that the strain and pendulum instruments have been matched in amplitude. Figure 6 is the comparative beam response with one element (No. 2) of the TFO array eliminated.

Figure 7 is the beam response with three elements (Nos. 2, 5, and 6) eliminated. The response of the TFO array includes the cos α response of the horizontal instruments steered for a 235° azimuth event. The comparative 3 dB apertures of the beams are:

QCAZ	64°
TFO (six elements)	48°
TFO (four elements)	51°

At TFO, the long period instruments are used in this analysis. Radial and transverse components are computed

-3-

from the horizontal instruments for a given earthquake azimuth. Figure 8 is an example of the rotation output for three sites. The radial and transverse seismograms are designated R and T respectively. In this case the Love wave is well-defined on the transverse instrument at about 01 10 and the Rayleigh wave about three minutes later on the radial instrument. This visual test was used to verify that the proper relative weights (calibrations) were used when the instruments were rotated. The phased sum (PS) and the unphased sum (US) were computed for the available elements of the TFO array. A surface wave phase velocity of 3.5 km/sec was used to compute the phased sum. Because of the lower phase velocity, body waves are enhanced on the unphased sum and Rayleigh waves on the phased sum.

At QCAZ the weighted sum and difference of a horizontal pendulum and strain seismograph have been computed for comparison with the TFO phased sum. The weighting factor includes local phase velocity and calibration, and has been adjusted to obtain maximum cancellation of the back beam. Other procedures used on the QCAZ data are described in the results section.

The data from QCAZ were obtained during the latter part of May 1970, prior to the installation of the vertical strain instruments. Although one can in theory obtain an equivalent vertical strain by adding the outputs from two orthogonal horizontal instruments, this procedure has not been used in this report. There was considerable installation activity in the mine at the time, which apparently reduced data quality.

The above discussion of beam comparison and QCAZ vs TFO has its first application to surface waves. The combination of strain and pendulum instruments can also be used to recognize and enhance body waves. The formulae for a homogeneous half-space relating strain and pendulum displacement involve the angle of

incidence of the particular body wave, the elastic parameters of
the medium, the horizontal component of phase velocity, and the
wavenumber (Appendix II). Experience obtained in the application
of these formulae at various strain sites is that they are
principally useful to establish phase relations.

Romney (1964) derives the relation

$$\frac{\partial u_x}{\partial x} + \frac{\partial u_y}{\partial y} = -\frac{\lambda+2\mu}{\lambda}\frac{\partial u_z}{\partial z}$$

which says that the sum of the horizontal strains is equal to a
constant times the vertical strain. This equation, which also
assumes homogeneity, can be used to estimate the ratio $(\lambda+2\mu)/\lambda$.
Applying this equation to WMO data, we found that $\lambda = 2\mu$
is a better approximation than the usual assumption $\lambda = \mu$. At
the present time such data are not available at QCAZ.

Strain-pendulum combinations can also be used to determine
local phase velocity for a dispersed surface wave train. The
technique consists of measuring the relative amplitude and period
of each half-cycle. Amplitudes are measured only at the peaks and
troughs of the waves to avoid the inaccuracy involved in comparing
the ratios of small numbers. The mathematical justification for
this procedure is included in the Discussion of Results. Mikumo
and Aki (1964) determined local phase velocity by this method,
using the strain installation at Isabella, California.

-5-

DISCUSSION OF RESULTS

QCAZ-TFO comparison

Seven earthquakes recorded at QCAZ and TFO have been selected
to compare beam response. At QCAZ the beam is the sum or differ-
ence of the horizontal long-period strain and pendulum seismo-
graphs. At TFO the beam is the phased sum of the steered long-
period seismographs. USC&GS data for the earthquakes are listed
in Appendix I.

The ratio of signal amplitude to rms amplitude of the noise
is computed for one of the comparative beam response studies; the
high level of non-stationary noise gave unsatisfactory results
for other examples tried.

Figure 9 compares the QCAZ and TFO beams for an earthquake
off the coast of Chiapas, Mexico, on 19 May 1970. P, S and the
Rayleigh wave (LR) have been marked. For this earthquake,
southeast of QCAZ, the sum of the strain and pendulum
seismographs should enhance these phases. Channels 1, 3
and 4 at TFO are the same data used in the example describing
the rotation procedure (Figure 8). P and S are marked on the
unphased sum at TFO. At the scale of these plots, the travel
time differences across TFO for P and S are negligible. Examples
of the non-stationary noise are enclosed in a dashed-line block.

Figure 10 shows a 19 May 1970 earthquake from the Fiji Islands
region; only the Rayleigh wave has been identified. The path for
this earthquake is largely oceanic. The Chiapas earthquake (
(Figure 9) has a continental path. The surface waves from a
Greenland Sea earthquake occur prior to the Fiji earthquake
surface waves. The azimuth of this event falls outside the beam
at QCAZ; thus the sum and difference for this segment of data
has not been computed.

Figures 11 and 12 consist of two presentations of the QCAZ and TFO data for overlapping signals from three earthquakes. This is the type of data one wishes to have in order to further evaluate the two systems; the search for better examples is continuing. There are two Chiapas earthquakes; a small one followed about six minutes later by the magnitude 4.6 earthquake listed in Appendix I. The third earthquake is from the New Hebrides region. Travel time table analysis shows that several body wave phases from the New Hebrides earthquake should occur at nearly the same time as the surface waves from the Chiapas earthquakes. In Figure 11, both QCAZ and TFO are beamed to the southeast. The only well-defined phase is the Rayleigh wave from the second (larger) Chiapas earthquake; other tentative identifications have been made.

Figure 12 shows the same data as Figure 11 except that here the 55° azimuth strain and pendulum at QCAZ have been used. TFO has again been beamed to the southeast, but the horizontal instruments have been rotated to obtain a radial component directed to the southwest (New Hebrides). At QCAZ the Love waves from Mexico should be well recorded only on the 55° pendulum instrument. Both the strain and pendulum instruments should record body wave phases from the New Hebrides earthquake, and these should be enhanced on the sum channel. Phases marked on the QCAZ sum channel (S55 plus P55) occur at the time computed from the Jeffreys-Bullen travel-time curves. The TFO sample includes body wave phases from the New Hebrides and the Love waves from Chiapas. Body wave phases should be enhanced on the unphased sum. In computing the phased sum travel time delays for surface waves from the southeast have been used. Thus the Love waves from Chiapas should be enhanced on the phased sum, because the transverse Love wave component is approximately aligned with the radial instruments steered southwest.

Figure 13 is the QCAZ-TFO comparison for a Kermadec Islands earthquake on 25 May 1970. A number of body wave phases have been identified in addition to the Rayleigh wave.

As a means of comparing the opposite azimuth cancellation obtained for the QCAZ data, the earthquake data of Figure 13 (Kermadec Islands) has been steered toward the opposite azimuth. The phased sum of Figure 14 should be compared with the difference channel (S55 - P55) of Figure 13.

Figure 15 is the QCAZ-TFO comparison for an earthquake south of Panama. In this case there is a substantial character difference in the Rayleigh wave between QCAZ and TFO.

In order to obtain a numerical comparison of the effectiveness of the beam-forming at QCAZ and TFO, a signal and a noise sample have been selected. The signal data used are from the Fiji earthquake of 19 May 1970 (Figure 10). The non-stationary noise on the strain instrument at QCAZ and on the horizontal pendulums at TFO restricted the choice of noise samples. The noise sample selected consists of 500 seconds, beginning 1050 seconds after the beginning of the data sample of Figure 10. It thus occurs after the Rayleigh wave from the Greenland Sea earthquake and prior to the noise on the TFO 5R instrument. Figures 16 and 17 are plots of the noise samples used as recorded on the horizontal instruments. Figure 16 is selected from TFO and Figure 17 is the corresponding sample selected at QCAZ. At QCAZ the gains have been adjusted so that the Rayleigh wave amplitudes are equal on the strain and pendulum seismographs. This amounts to compensating for the average local phase velocity (Figure 10). Visual inspection of the noise samples indicates that the sample selection has fulfilled its purpose by avoiding the Rayleigh wave from the Greenland Sea earthquake and the non-stationary noise which occurs at both sites.

The sample has been filtered with a 15 to 50 second band-pass filter.

The following signal to rms noise ratios for the Fiji earthquake were obtained for sum and difference of the horizontal instruments at QCAZ and the horizontal and vertical instruments at TFO. Figure 18 is a plot of the beamed vertical long period instruments.

QCAZ Data	S/rms	db
S55L (Horizontal strain 55° azimuth)	10.16	20.9
P55L (Horizontal pendulum 55° azimuth)	11.0	20.9
SUM (S55L + P55L)	15.0	23.5
DIF (S55L-P55L)	4.0	12.0

TFO Data	Radial		Vertical	
Channel No.	S/rms	db	S/rms	db
1	10.35	20.3	8.64	18.7
3	8.19	18.3	12.28	21.8
4	5.87	15.4	10.49	20.7
5	4.66	13.4	4.57	13.2
6	--	--	5.17	14.3
7	4.49	13.0	8.41	18.5
Mean	6.71	16.5	8.26	18.3
Unphased Sum	3.14	9.9	4.40	12.9
Phased Sum	6.45	16.2	17.71	25.0

Thus the SUM channel at QCAZ has 1.5 db less signal to noise improvement than the phased sum of the vertical instruments at TFO and 7.3 db greater signal to noise improvement than the phased sum of the radial instruments. At QCAZ the SUM channel is 2.6 db better than the radial pendulum (S55L). It seems likely that the results for the TFO radial instruments is anomalous. The S/rms ratio of the phased sum is 0.3 db less than the mean. Among known problems are a ratner high level of

uncertainity in the calibrations, the non-stationary noise and the possible error from merging two seismograms.

Enhancement of transverse waves

The Greenland Sea earthquake of 19 May 1970 has an azimuth at QCAZ of 11.3° (the installed azimuths of the horizontal strain seismographs are 55° and 325°) which is such that SH and Love waves should be enhanced by the difference of the orthogonal horizontal strain seismographs.

Figure 19 shows the sum and difference of the horizontal strain seismographs at QCAZ during the expected arrival time of surface waves from the Greenland Sea earthquake. The computed arrival time of the Love wave has been marked. Computation was based on the Jeffreys-Bullen travel times. The surface wave arrivals, as interpreted, have been enclosed in boxes in the figure.

Determination of local phase velocity

Given a single Rayleigh mode whose horizontal component is defined by

$$u_x = g \, (k_n z) \sin (k_n x - \omega t)$$

the horizontal strain output with an electromagnetic transducer is

$$\frac{d}{dt} \frac{\partial u_x}{\partial x} = \omega k_n \, g(k_n z) \sin(k_n x - \omega t)$$

and the horizontal pendulum output is

$$\frac{d^2}{dt^2}(u_x) = -\omega^2 g(k_n z) \sin(k_n x - \omega t)$$

The ratio of strain to pendulum amplitude is

$$-\frac{\omega k_n}{\omega^2} = -\frac{k_n}{\omega} = -\frac{1}{c_n}$$

where c_n is the local phase velocity.

One can also show using a long algebraic argument that in a homogeneous half-space, the ratio of horizontal strain amplitude to horizontal pendulum amplitude is $1/c_n$ for both P and SV waves.

The application of these formulae requires that only a single type of wave or Rayleigh mode occur at any given record time. If one had two waves arriving simultaneously, such as S and PcS at $\Delta = 39°$, it would not be possible to determine phase velocity.

In computing local phase velocity, we identify the maximum and minimum value of each half cycle in the selected time period, measure the ratio of the strain and pendulum amplitudes at their maximum and minimum amplitude values, and plot the ratios against the corresponding half-period (times two).

Figure 20 shows the local phase velocity at QCAZ calculated

for detailed analysis. Figure 8 (previously described) is the
QCAZ-TFO comparison for this earthquake. The analog computer was
used in the present analysis; channel gains were adjusted to
obtain cancellation of the sum or difference. Figures 22 to 25
show the outputs of various instruments for selected time
segments of the Chiapas signal. An analog circuit to obtain
outputs phase-shifted 90° relative to each other has been used
as part of the analytical procedure.

Figure 22 shows the outputs of the radial long-period pen-
dulum, the vertical long-period pendulum and their sum and
difference, for the Chiapas earthquake. The calculated arrival
times of the phases P, S, and SS from the Jeffreys-Bullen
tables have been marked. There is an additional phase at about
01 03 45 that is not predicted by the travel time tables. The
S phase is 90° out of phase on the radial and vertical pendu-
lums. The ratio of displacement for a homogeneous half-space
is given by the formula

$$\frac{u_z}{u_x}\bigg|_{z=0} = \frac{2 \sin\phi [\mu/(\lambda + 2\mu) - \sin^2\phi]^{1/2}}{\sin 2\phi}$$

for SV waves incident at an angle ϕ (Appendix II). If $\lambda = \mu$,
the numerator becomes zero at 35.3°, where $\sin \phi = 1/3^{1/2}$.
For angles greater than ϕ, the ratio is imaginary, indicating
a 90° phase difference between the horizontal and vertical
pendulum for incidence angles greater than 35.3°. For the
Chiapas earthquake, using the slope of the travel time curve,
assuming a compressional velocity of 6.4 km/sec, and $\lambda = \mu$,

-13-

one obtains $\phi \simeq 34°$.

However the many assumptions in this calculation render the results suspect. For some fixed value of $\phi \geq 35°$

$$u_z = jK \, u_x$$

where $j = \sqrt{-1}$ and K includes all the constant terms. Thus u_z (vertical pendulum) is expected to lead u_x (horizontal pendulum) by 90°. This analysis of pendulum channels is included to support the data analysis of the strain-pendulum combinations.

Figure 23 shows the radial long-period pendulum and strain outputs, and their sum and difference. There is an apparent polarity reversal in the strain circuit. For this azimuth (133.1°) the sum should enhance S and Rayleigh waves. The computed travel time of S and the peak amplitude of the Rayleigh wave have been marked. There is apparent surface wave or body wave energy beginning about 01 11 30, as marked by an arrow. Prior to the marked time the difference cancellation is not as effective.

Figure 24 shows the vertical and horizontal pendulum outputs for the same time segment as Figure 23. An analog 90° phase-shift circuit has been applied, so that in the figure the outputs will be in phase or 180° out of phase. In this case S is enhanced on the difference and the Rayleigh waves on the sum channel. The retrograde motion beginning at 01 11 30 is nearly identical to that obtained from the strain-pendulum sum (Figure 23).

Figure 24 shows the transverse pendulum output (P55L) and the sum of the orthogonal horizontal strain outputs. The latter is equivalent to a vertical strain instrument. The peak of the Love waves, and an apparent SH component of S,

have been marked on the transverse pendulum. As expected, the Love wave at 0111 is not seen on the vertical pendulum output. The Love wave should also be enhanced on the difference of the orthogonal strain instruments, but in this example the signal-to-noise ratio is not actually improved over the transverse pendulum.

There is a phase that is enhanced on the sum with a peak about 01 12. Enhancement on the sum trace indicates that it is not SH-type motion. There is no well-defined evidence of its occurrence on the vertical pendulum. Such motion as is seen there is probably the early arriving Rayleigh wave.

The evidence is thus for the occurrence of a low-frequency (T ≃ 20 secs) wave whose principal motion is horizontal. It cannot be clearly identified as a Rayleigh or Love wave.

SUMMARY AND CONCLUSIONS

The beam comparisons between QCAZ and TFO are consistent
with the hypothesis that the signal enhancement of Rayleigh
waves for the two systems are approximately equal when system
noise is low. This hypothesis was investigated in detail for
one example in which it was possible to compare signal amplitudes
to the rms amplitude of the noise.

Love wave enhancement has been obtained using a technique
that is limited to signals whose azimuth from the station is
between about 30° to 60° from the installed azimuths of ortho-
gonal strain seismographs. In the example used both strain
channels had a high noise level.

A Chiapas earthquake has been examined in detail to
demonstrate signal enhancement techniques applied to P, S,
SH, Love, and Rayleigh waves.

Some preliminary data on use of the strain-pendulum ratio
to determine local phase velocity has been included.

These results show that the strain seismograph, in conjunc-
tion with a pendulum seismograph, can be used to form beams at
a single site, and that the combination can be used to enhance
and recognize the total seismic signal.

At the time this data was obtained, the instruments were
still in the process of being installed. Later data should
be free of some of the non-stationary noise that prevented a
more complete analysis at this time.

REFERENCES

Benioff, H., 1935, A linear strain seismograph: Bull. Seism. Soc. Amer., v. 25, p. 283-309.

Benioff, H., 1962, The characteristics of strain and pendulum seismograph combinations: in Proceedings of the Colloquium on Detection of Underground Nuclear Explosions: Vesiac Special Report, University of Michigan, Ann Arbor, Michigan.

Ewing, W.M., Jardatsky, W.S., and Press, F., 1957, Elastic waves in layered media: New York, McGraw-Hill Book Co., Inc.

Fix, J.E., and Sherwin, J.R., 1970, A high-sensitivity strain inertial seismograph installation: Technical Report No. 70-3, Teledyne Geotech, Garland, Texas.

Gupta, I., 1966, Response of vertical strain seismometer to body waves: Bull. Seism. Soc. Amer., v. 56, p. 785-791.

Jaeger, J.C., 1956, Elasticity, fracture, and flow (second edition): London, Methuen and Co. Ltd.

Mikumo, T., and Aki, K., 1964, Determination of local phase velocity by intercomparison of seismograms from strain and pendulum instruments: J. Geophys. Res., v. 69, p. 721-731.

Oliver, J., 1961, On the long period character of shear waves: Bull. Seism. Soc. Amer., v. 51, p. 1-12.
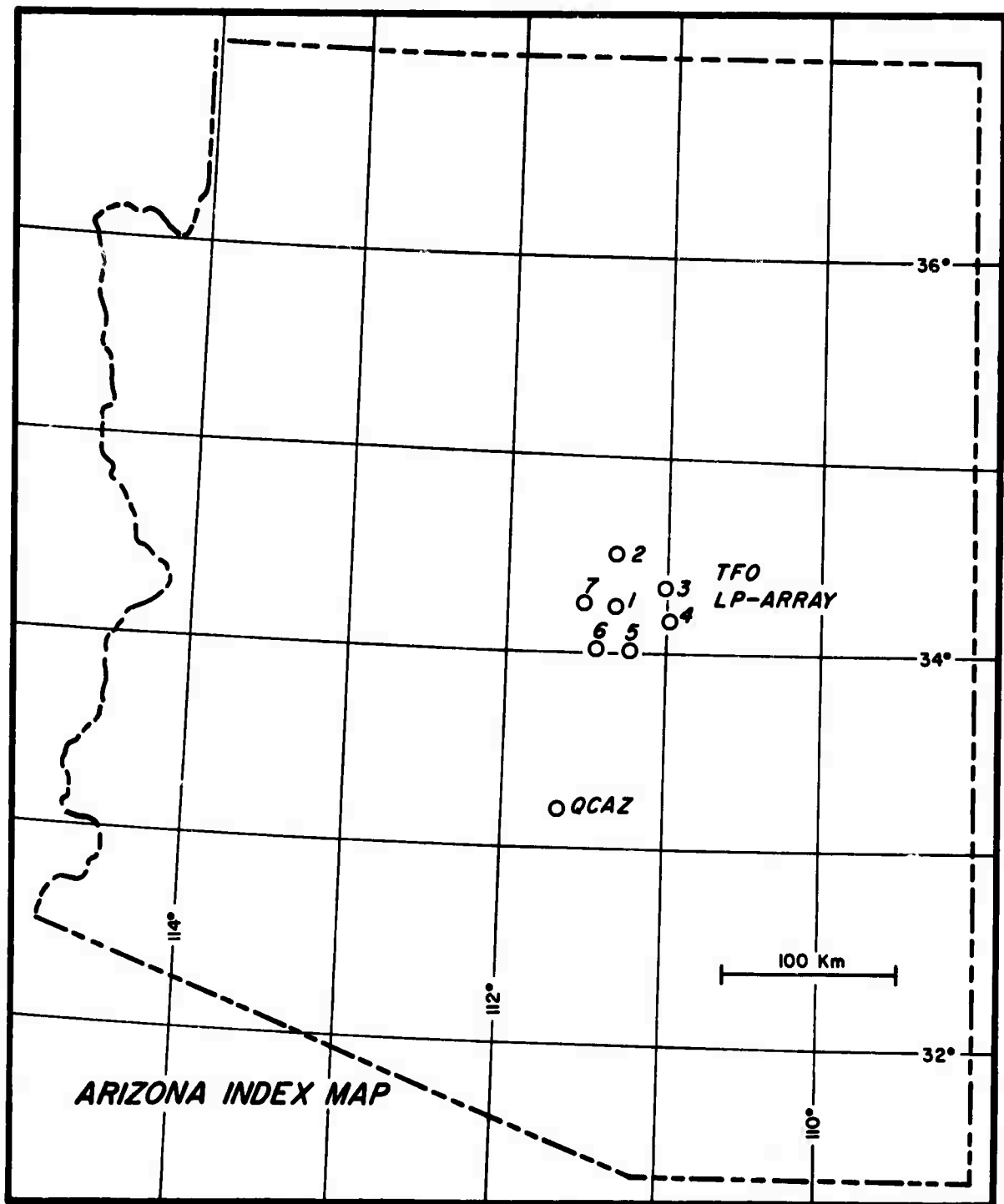
Figure 1. Arizona index map.

18
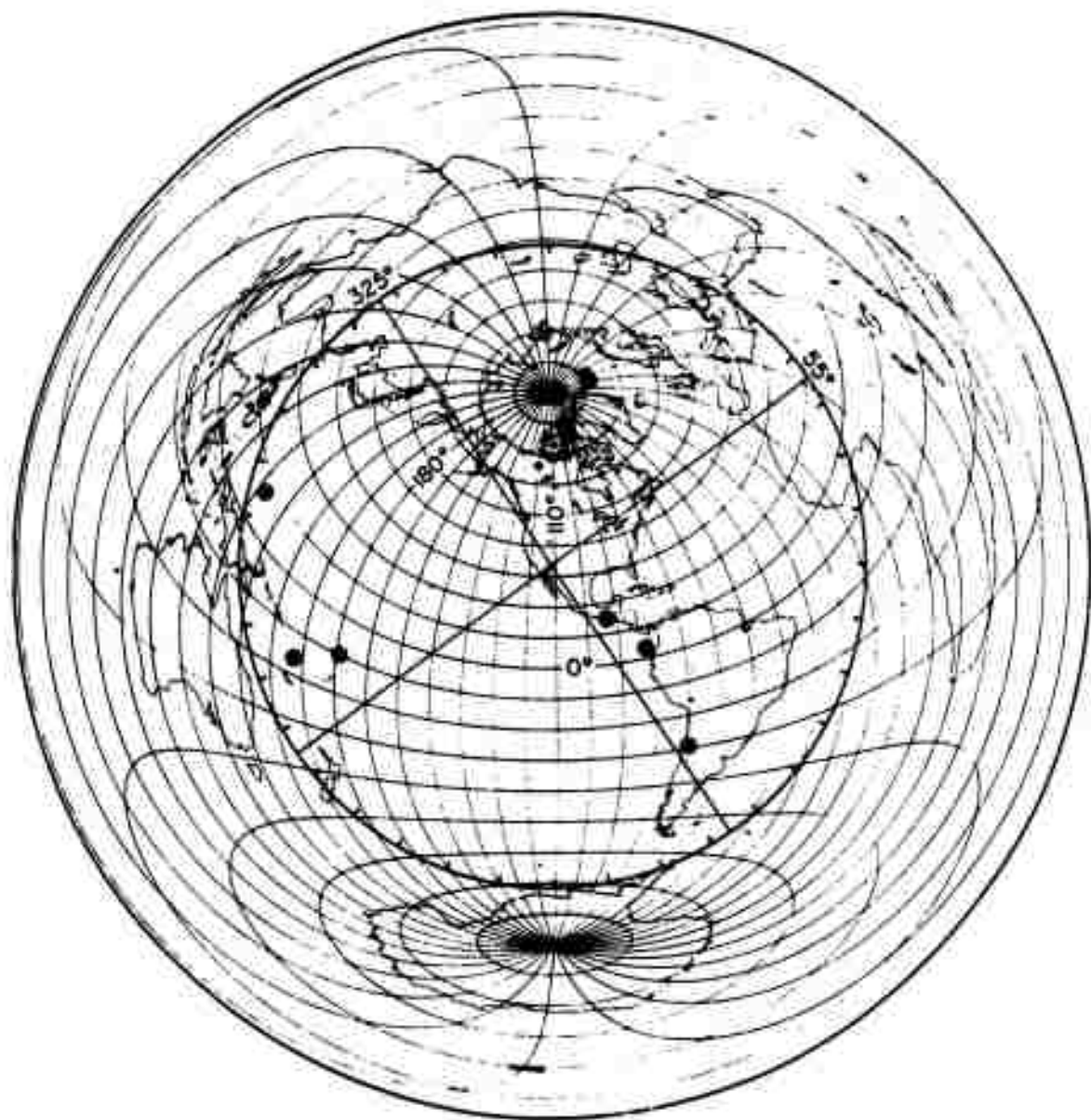
Figure 2. Location of earthquakes analyzed
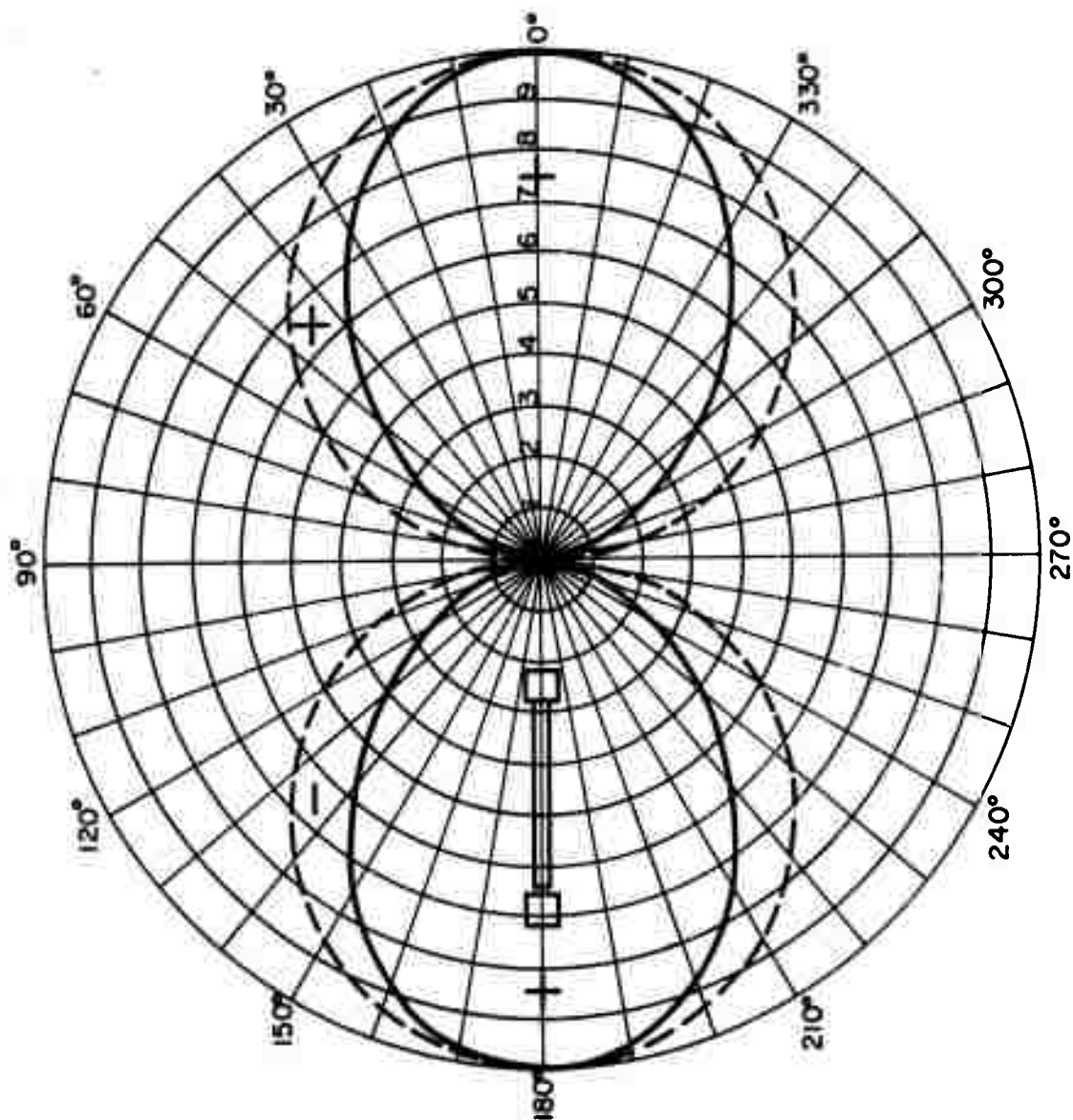
Figure 3. Azimuthal response of strain seismograph and horizontal pendulum seismograph to longitudinal plane waves or Rayleigh waves.

20
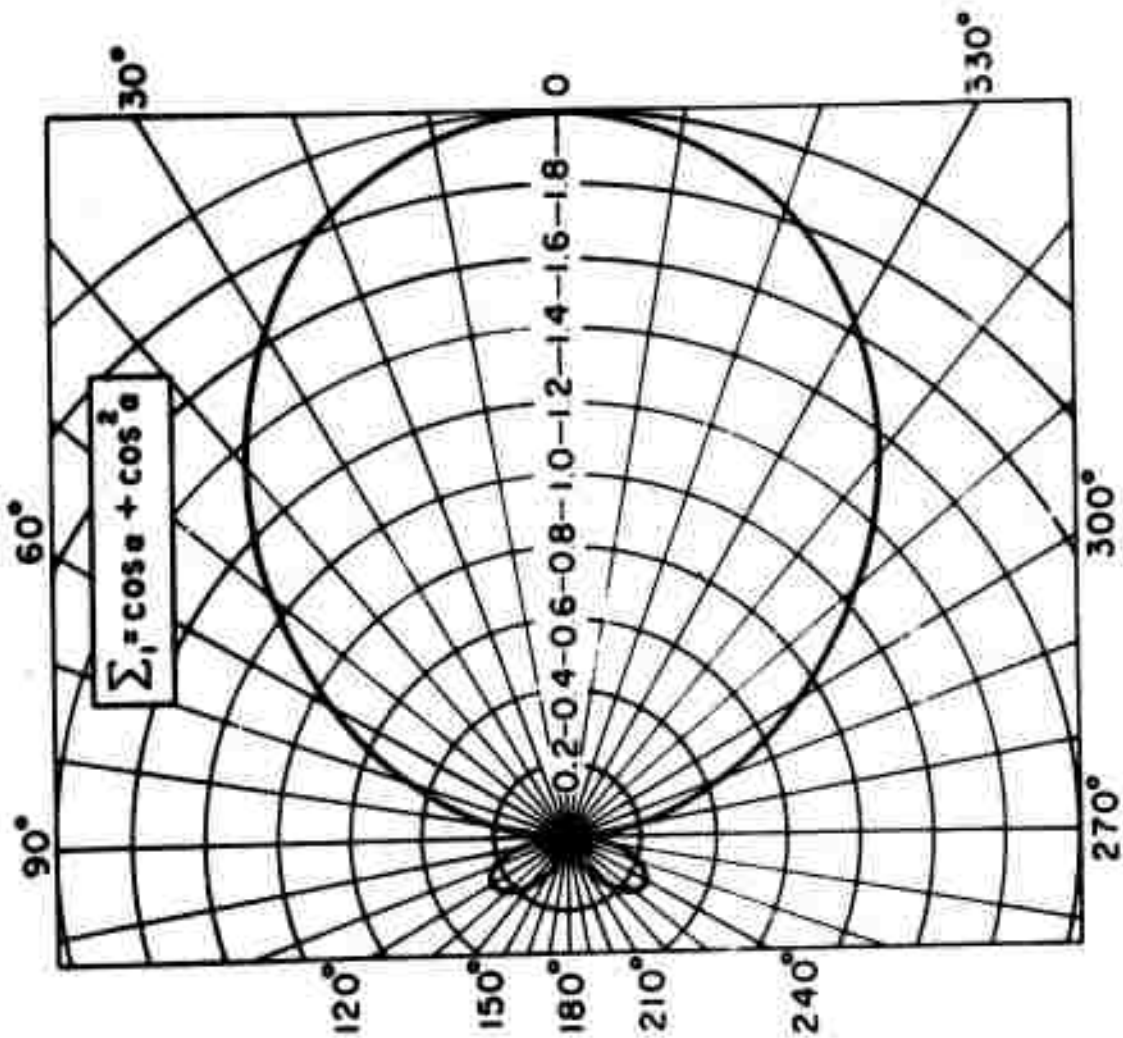
Figure 4. Sum response of horizontal strain and pendulum seismographs illustrated by Figure 3.

21
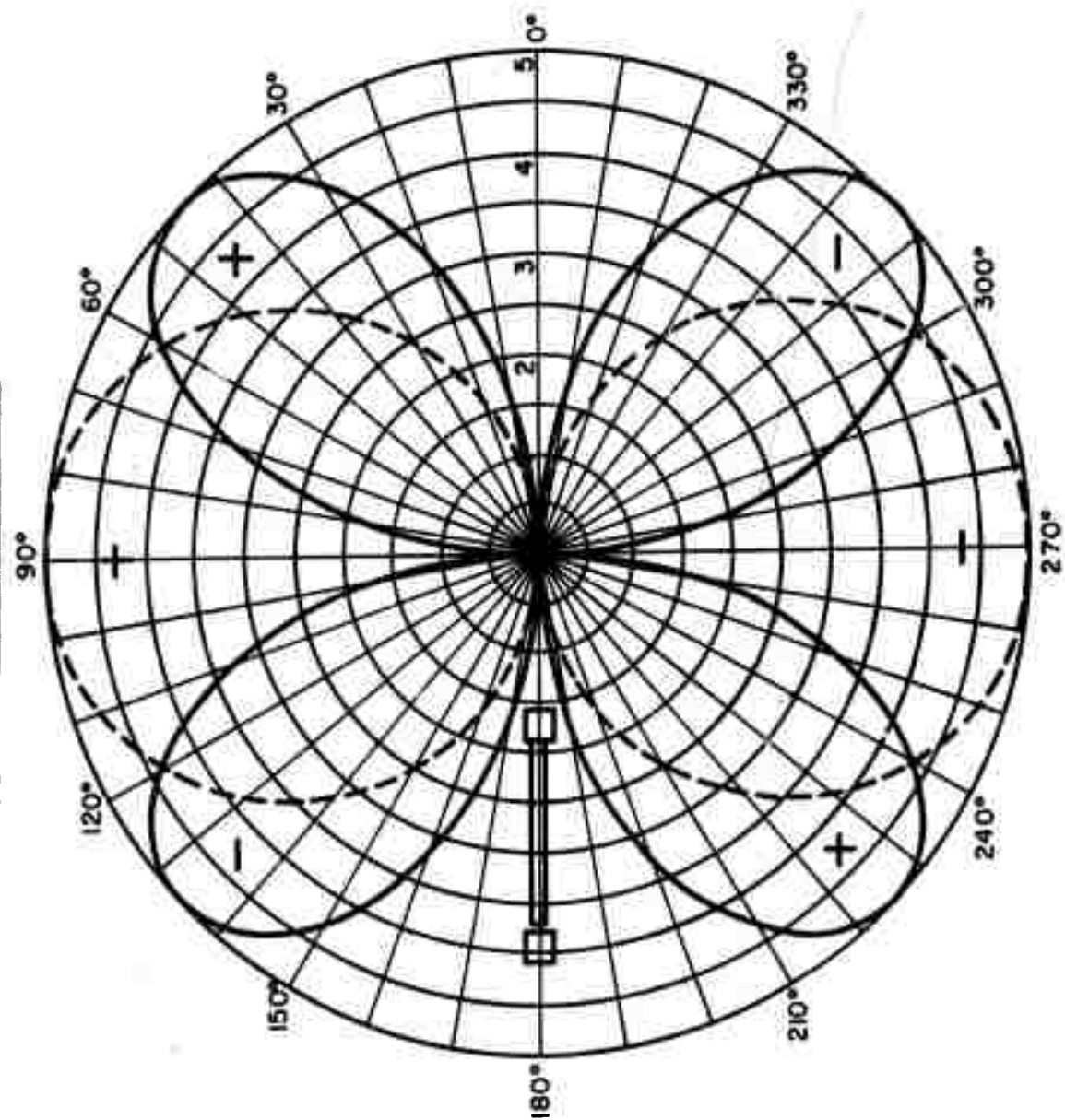
Figure 5. Response of horizontal strain seismograph to transverse waves (SH or Love).

22
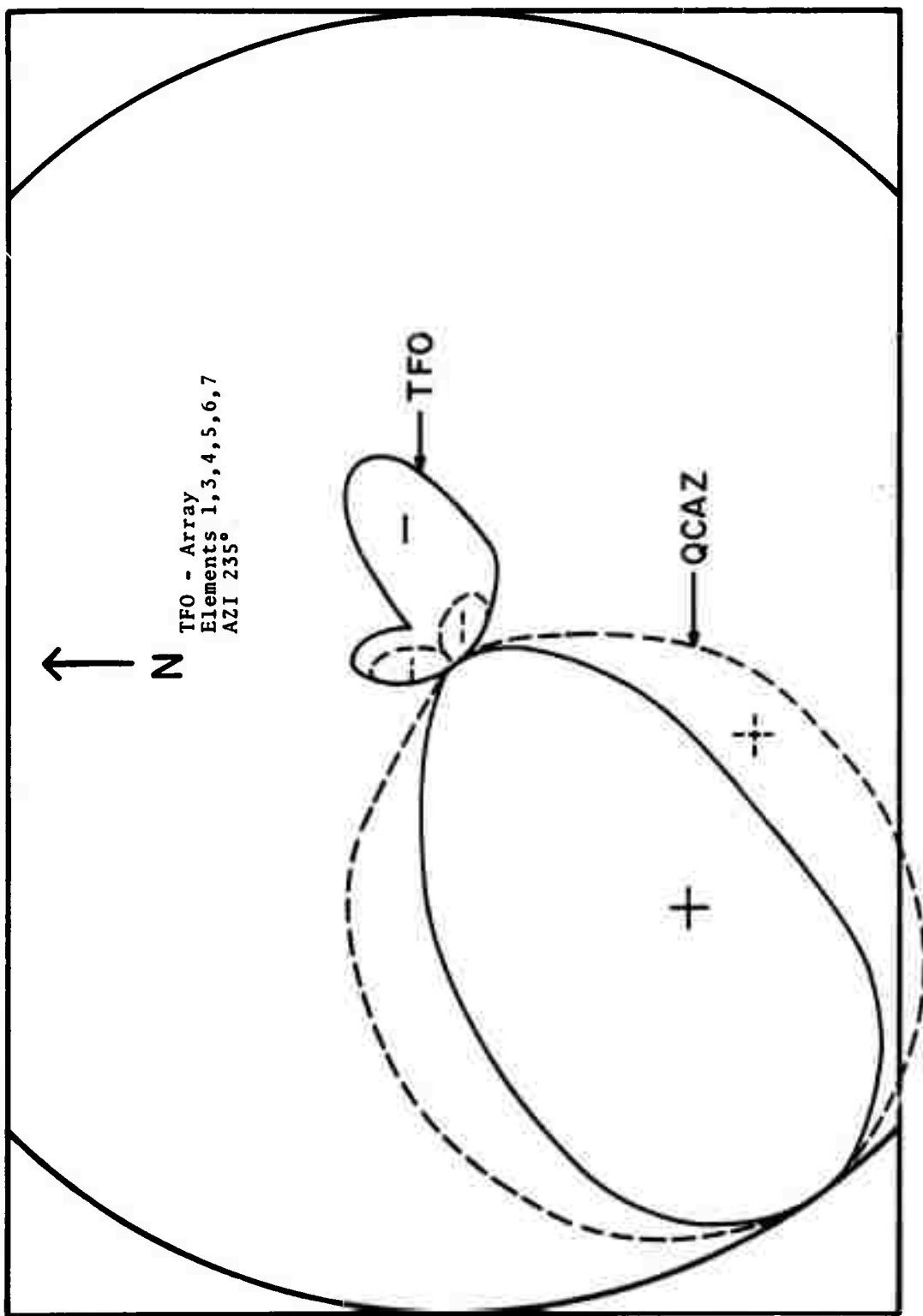
Figure 6. Beam pattern comparison TFO (6 elements) to QCAZ (sum of strain and pendulum)

23
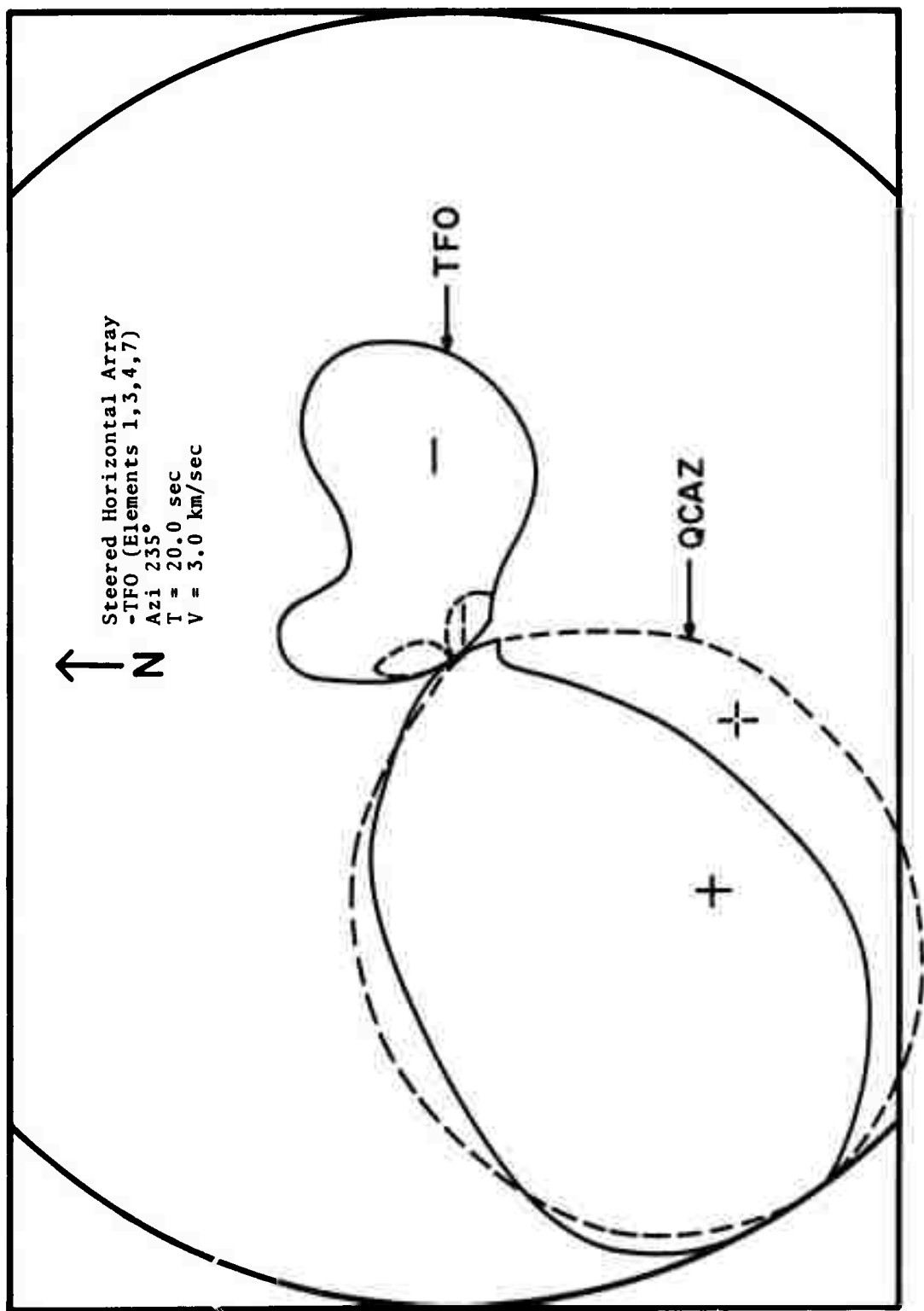
Figure 7. Bean pattern comparison TFO (4 elements) to QCAZ (sum of strain and pendulum).

Steered Horizontal Array
-TFO (Elements 1,3,4,7)
Azi 235°
T = 20.0 sec
V = 3.0 km/sec

N

TFO

QCAZ

EXAMPLE
HORIZONTAL ROTATION
AT TFO
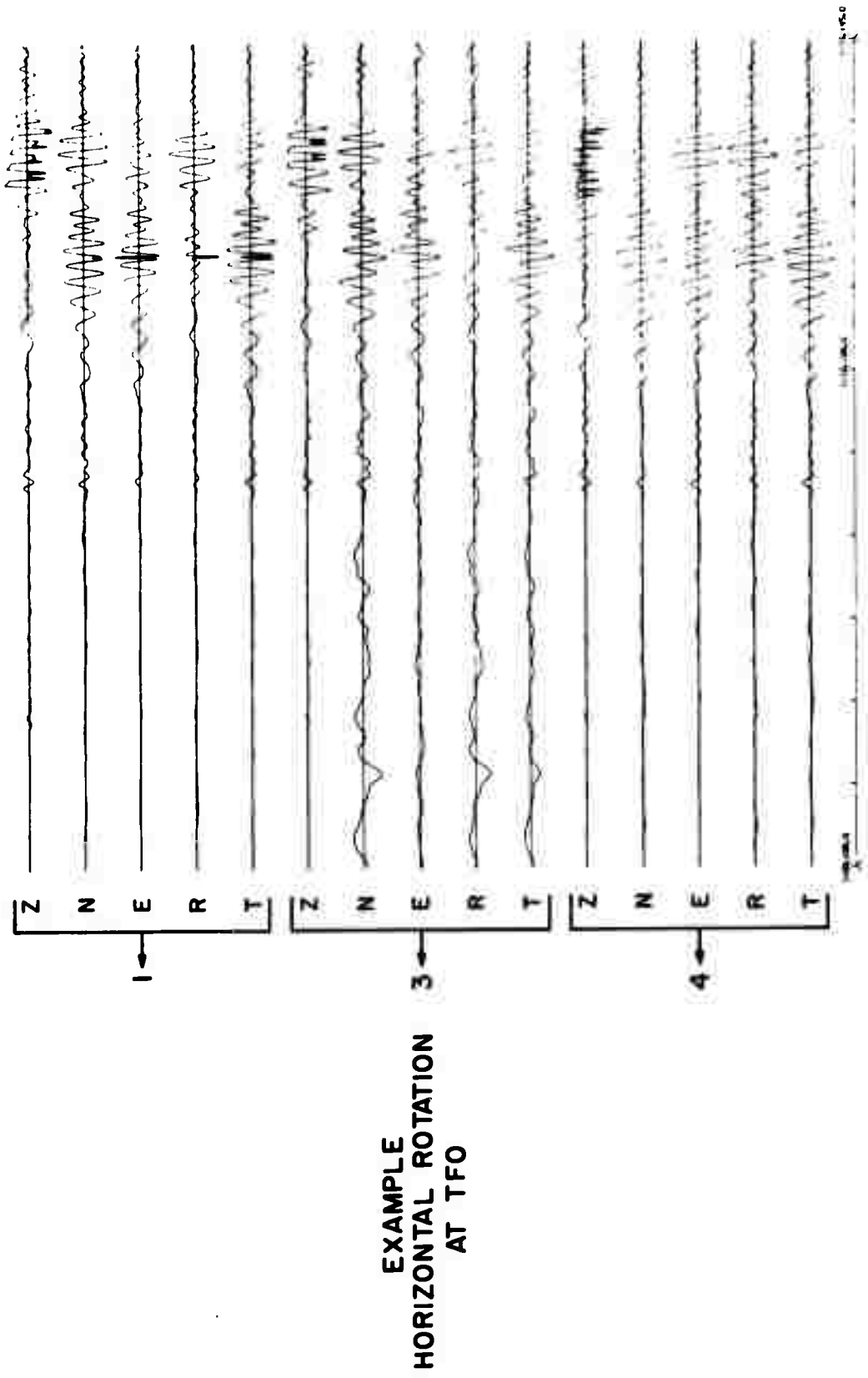
Figure 8. Example of horizontal rotation at TFO.

25
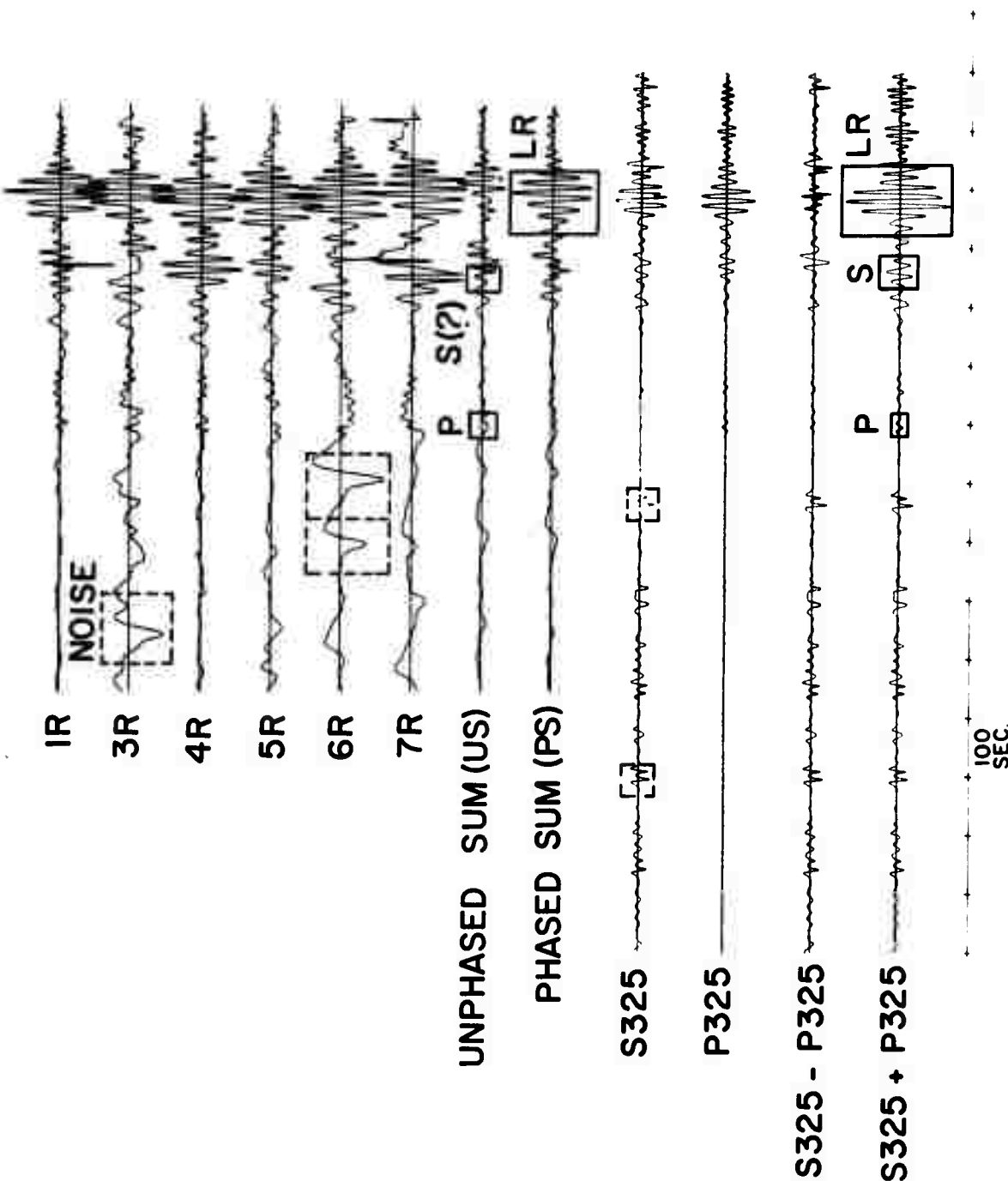
Figure 9. QCAZ-TFO comparison -- near Coast of Chiapas, Mexico, 19 May 1970.

26
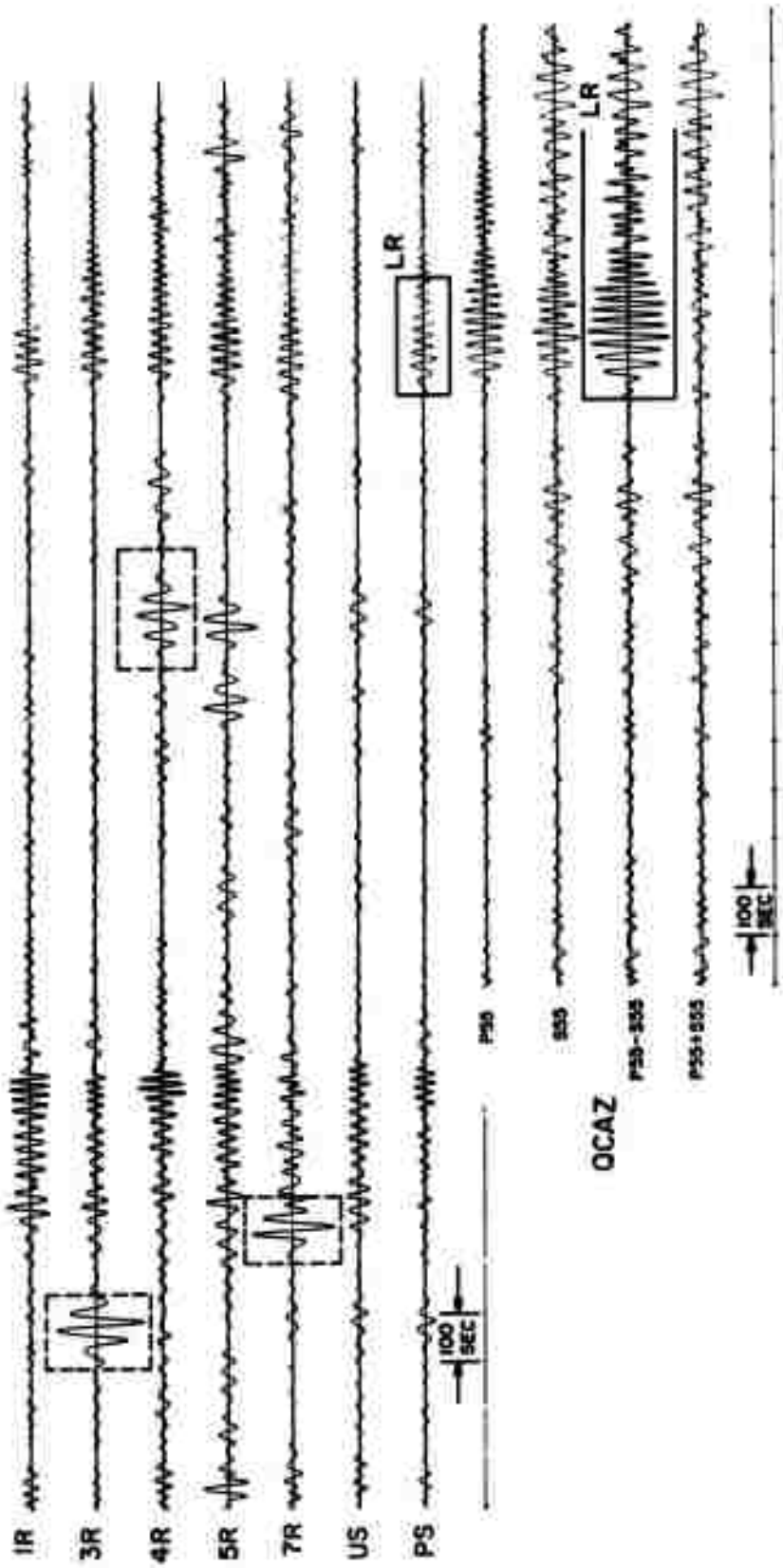
Figure 10. QCAZ-TFO comparison -- Fiji Islands 19 May 1970.
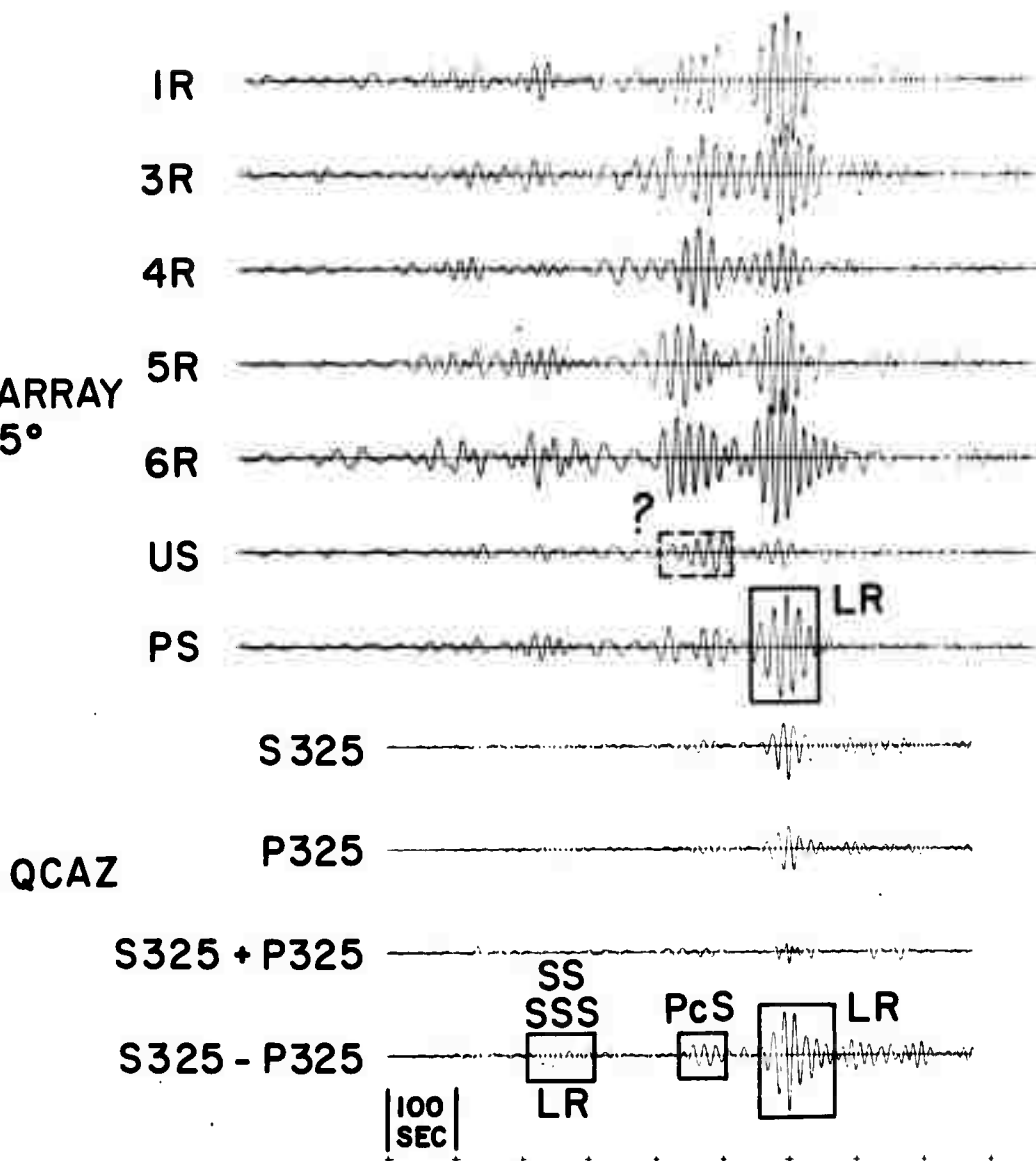
Figure 11. QCAZ-TFO comparison -- near Coast of Chiapas, Mexico, 21 May 1970.
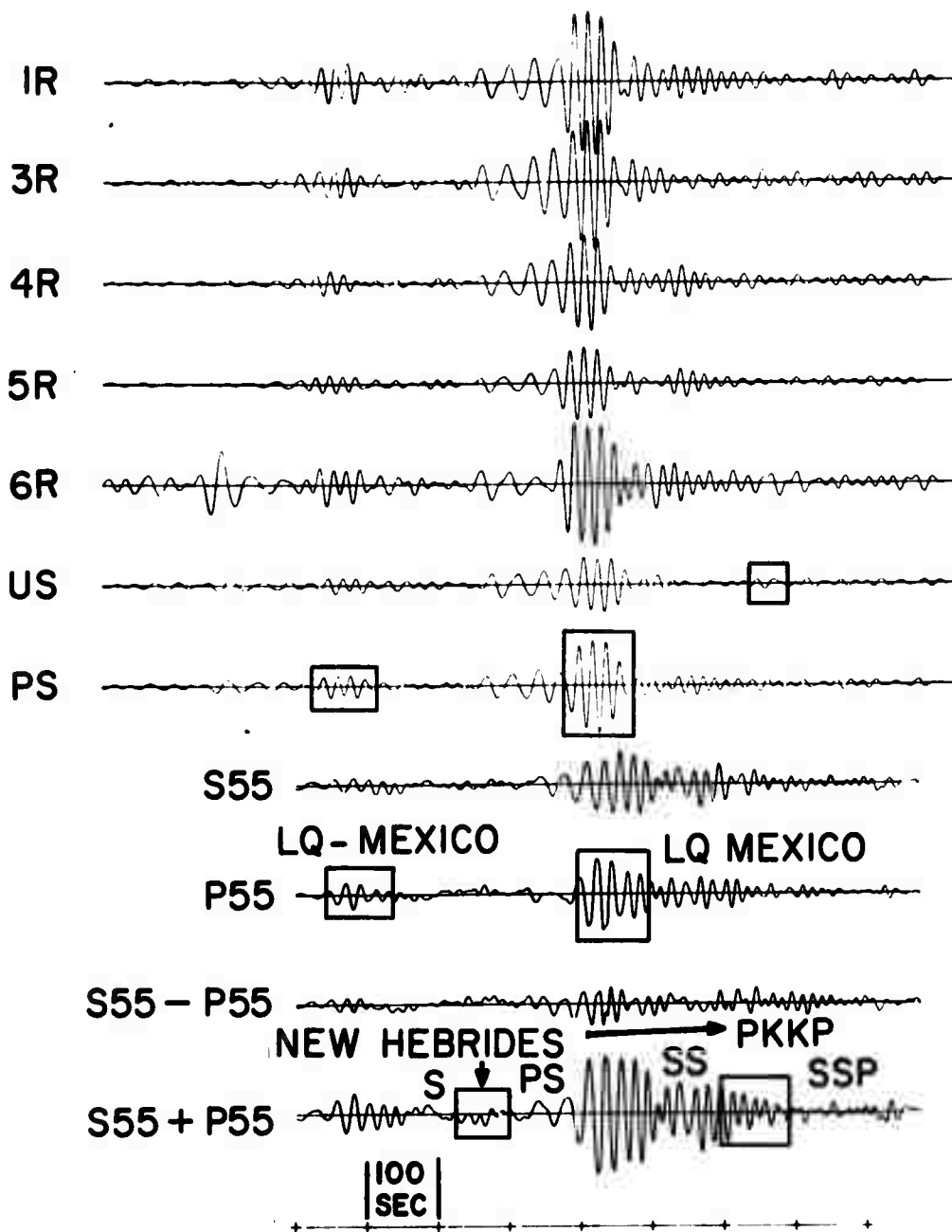
28

Figure 12. QCAZ-TFO comparison -- New Hebrides Islands,
21 May 1970.
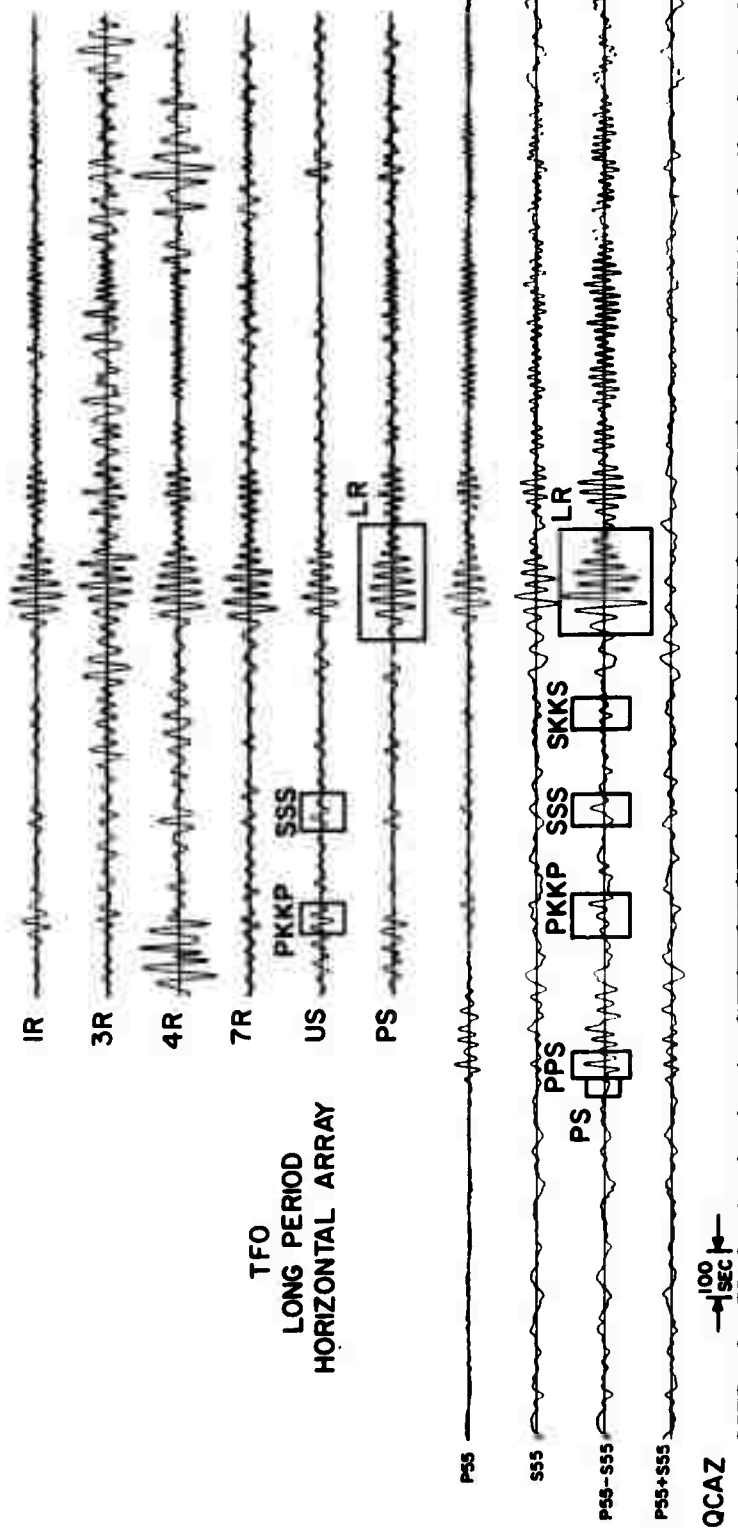
Figure 13. QCAZ-TFO comparison -- Kermadec Islands, 25 May 1970.
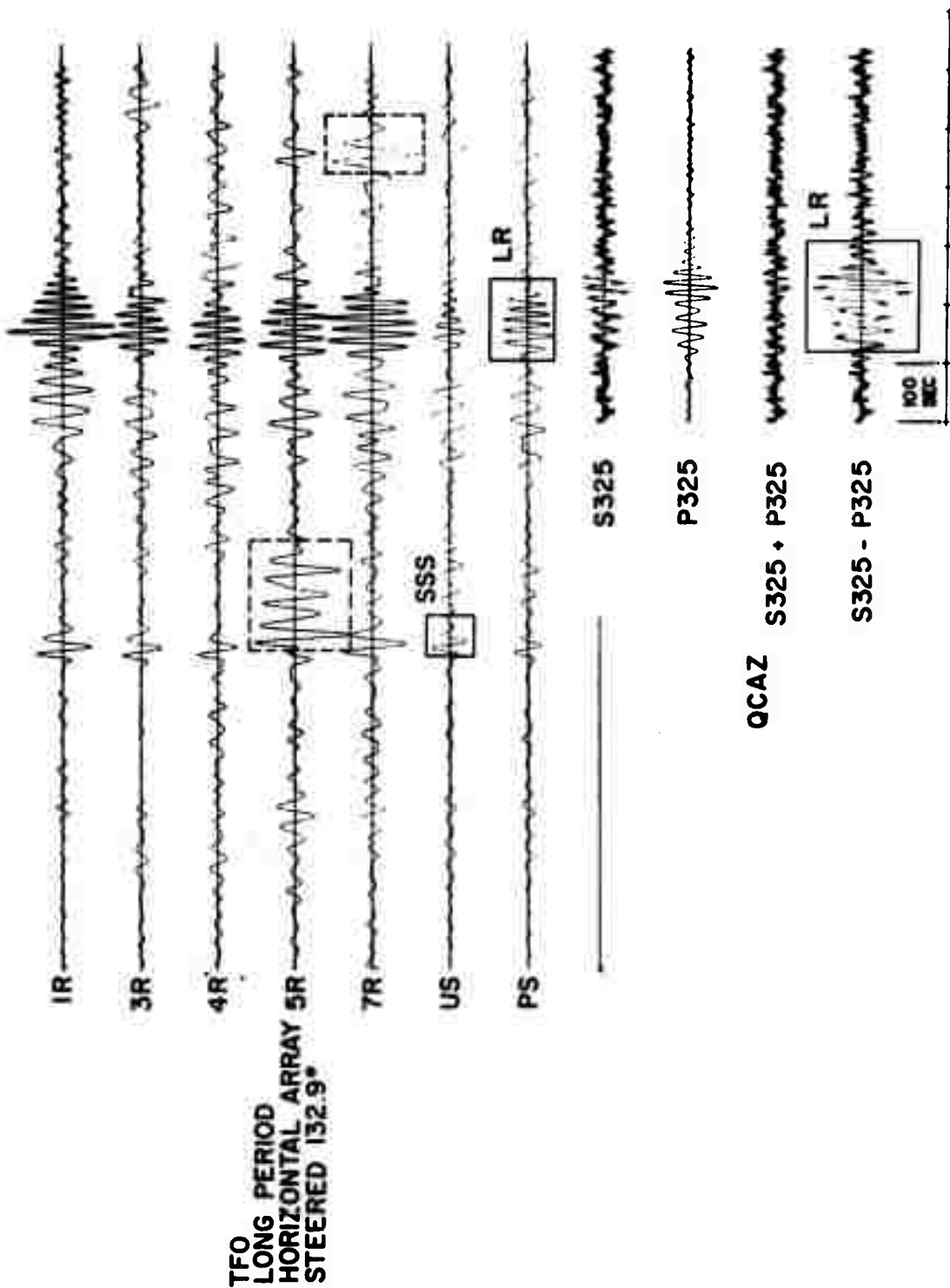
30
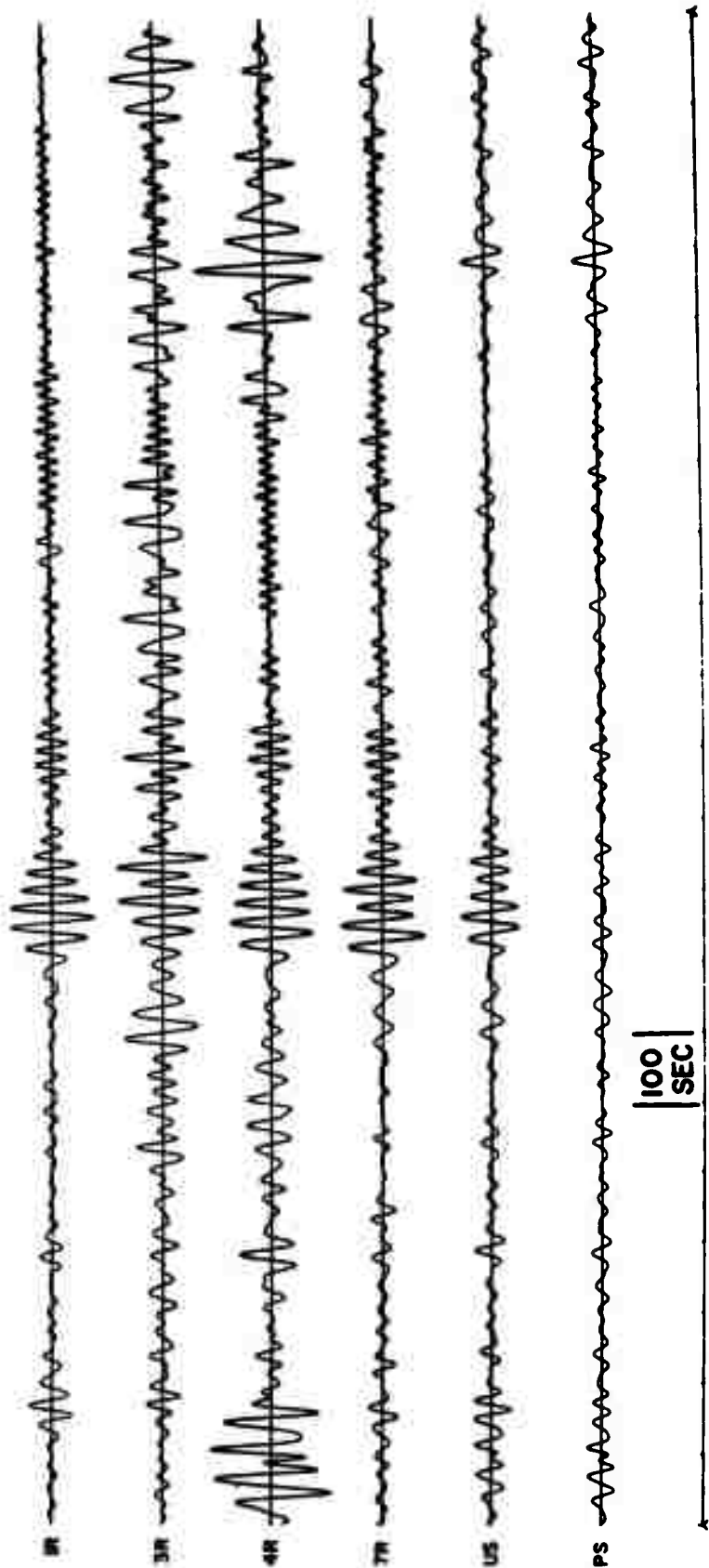
Figure 14. TFO back azimuth beam, Kermadec Islands, 25 May 1970.

31

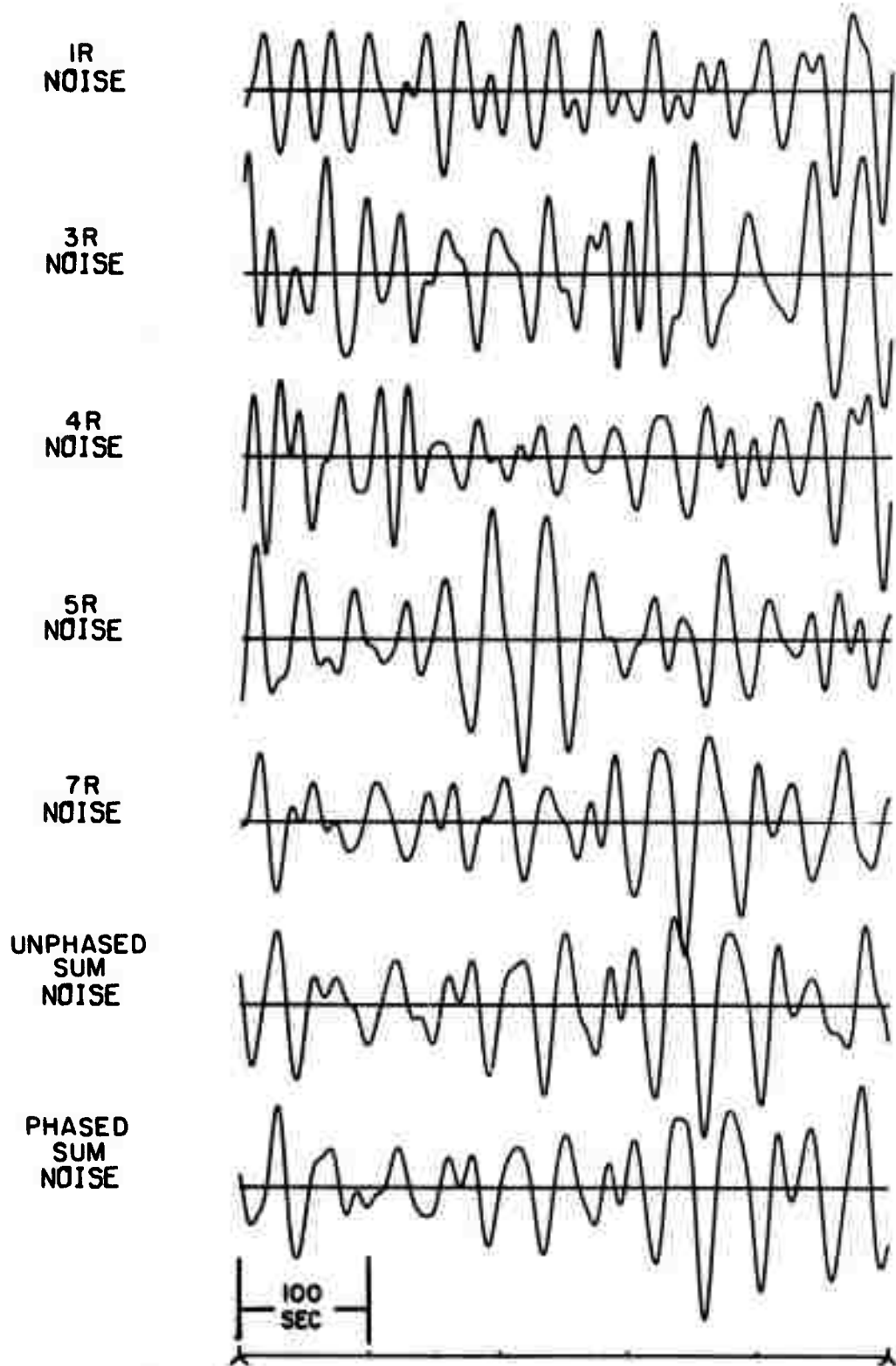Figure 15. QCAZ-TFO comparison south of Panama, 22 May 1970.

32

IR NOISE

3R NOISE

4R NOISE

5R NOISE

7R NOISE

UNPHASED SUM NOISE

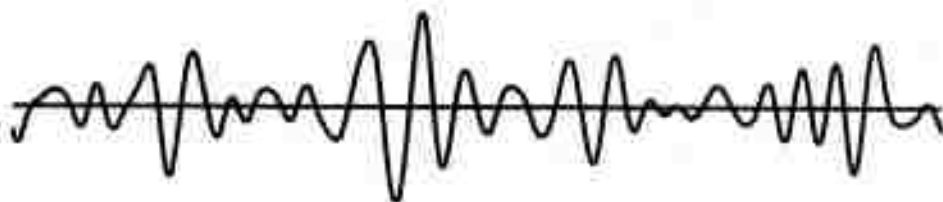PHASED SUM NOISE

100 SEC

Figure 16.   TFO -- noise sample, 19 May 1970.

33

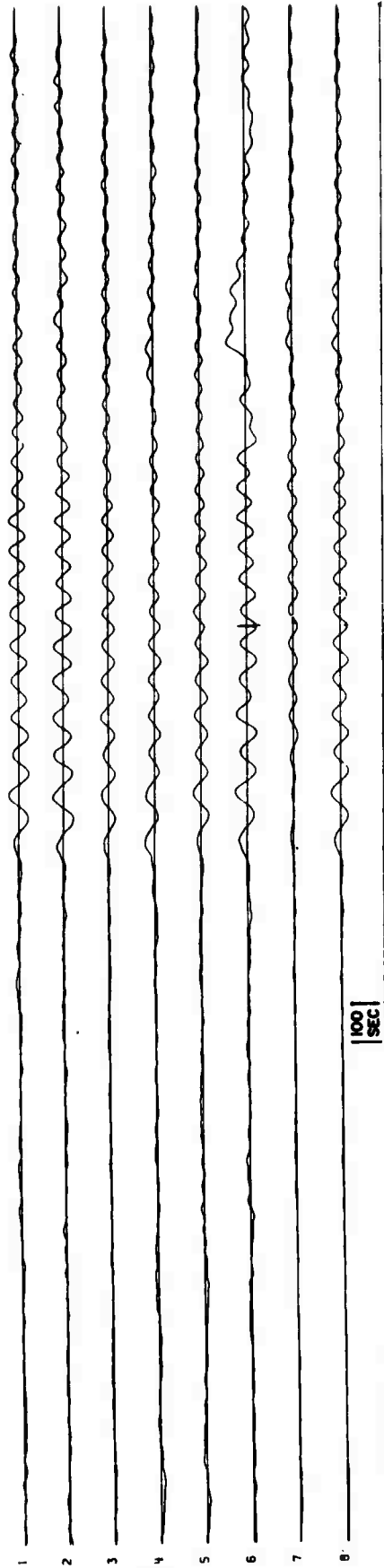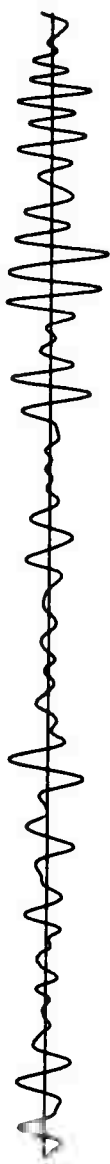Figure 17.   QCAZ -- noise sample, 19 May 1970.

34

Figure 18. TFO long period vertical array-
Beamed for 19 May 1970 Fiji Earthquake.
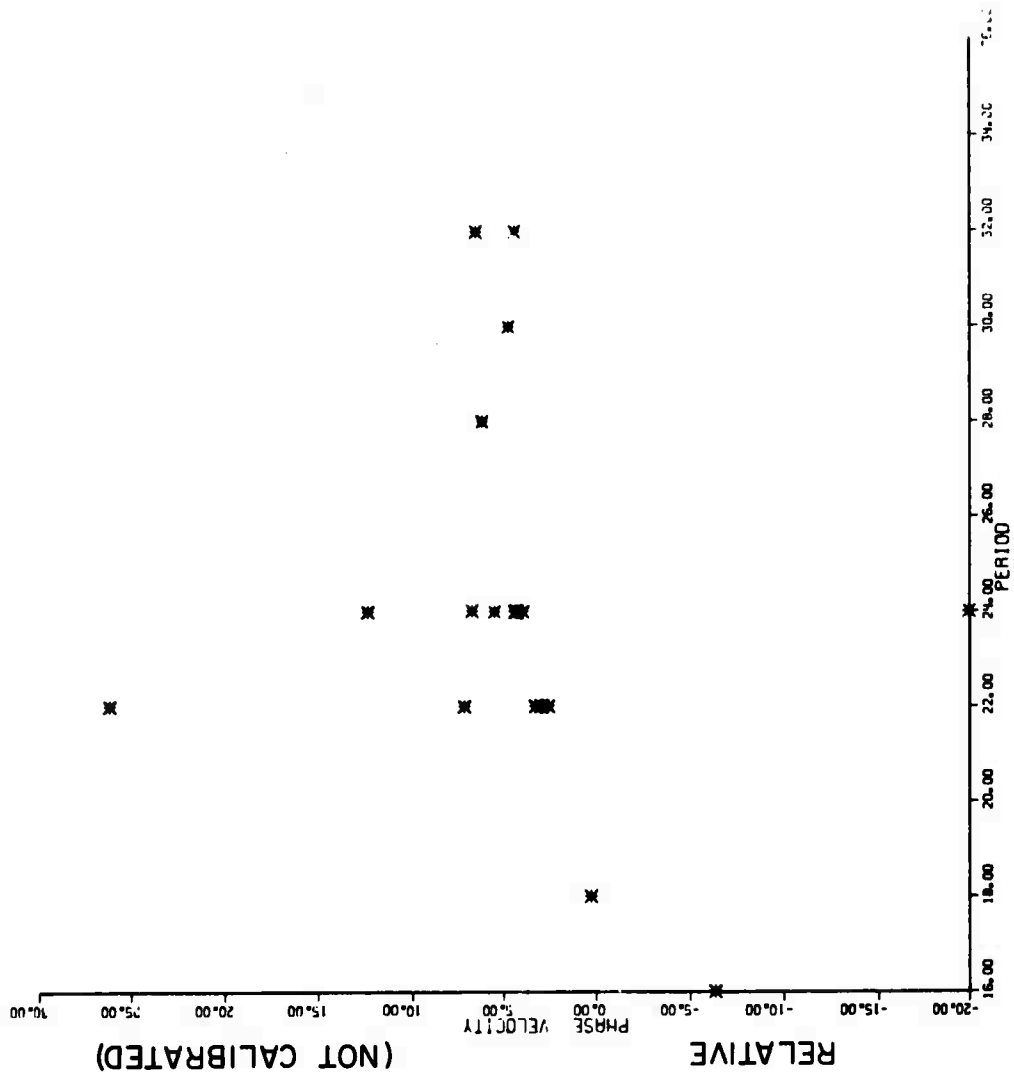
35

SS5

S32

SS5 + S32

SS5 − S32

COMPUTED
ARRIVALS

LQ   LR

Figure 19. Surface waves Greenland Sea earthquake, difference
of orthogonal horizontal strain to enhance Love waves.

36

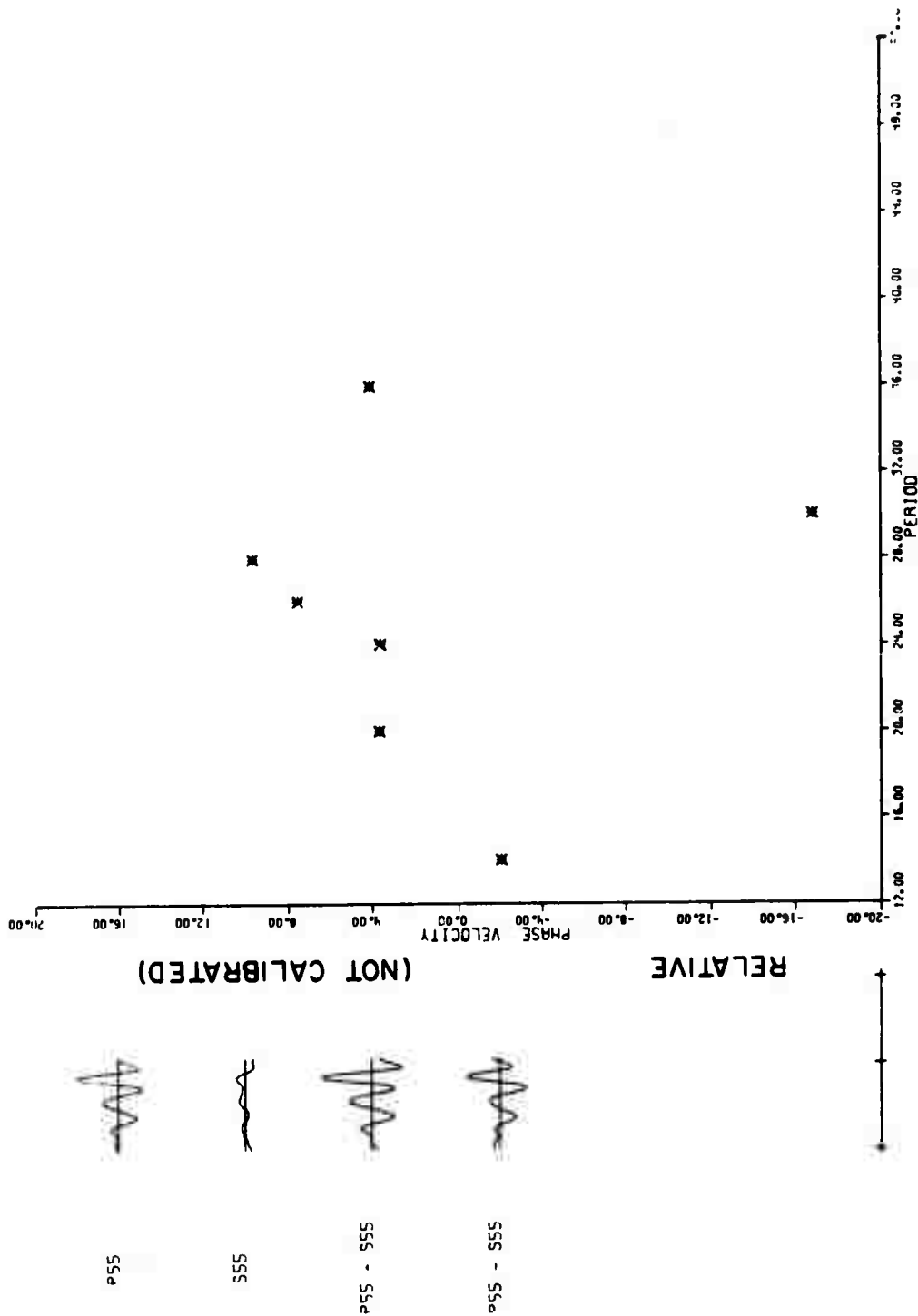Figure 20. Local phase velocity (Rayleigh) Kermadec Islands earthquake.

37

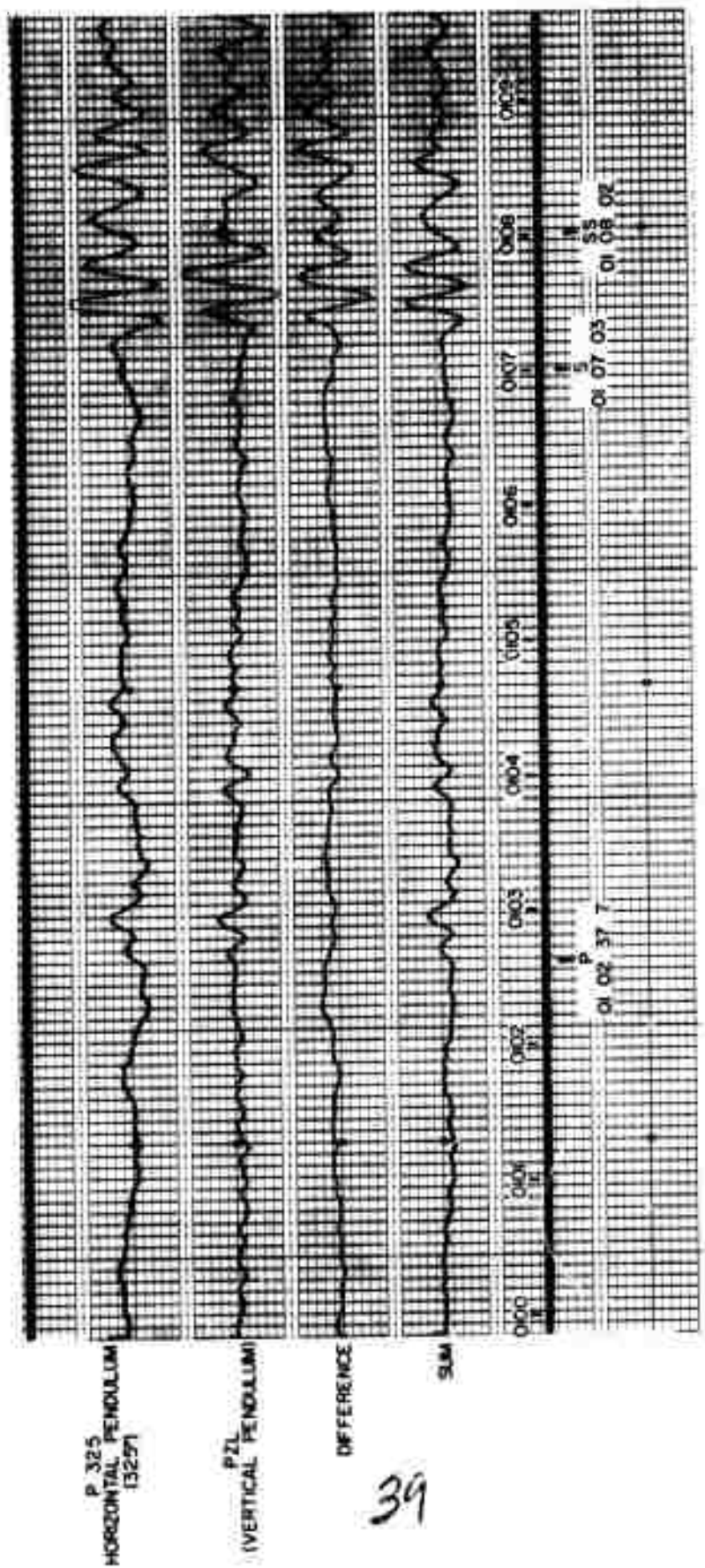Figure 21. Local phase velocity (PKKP) Kermadec Islands earthquake.

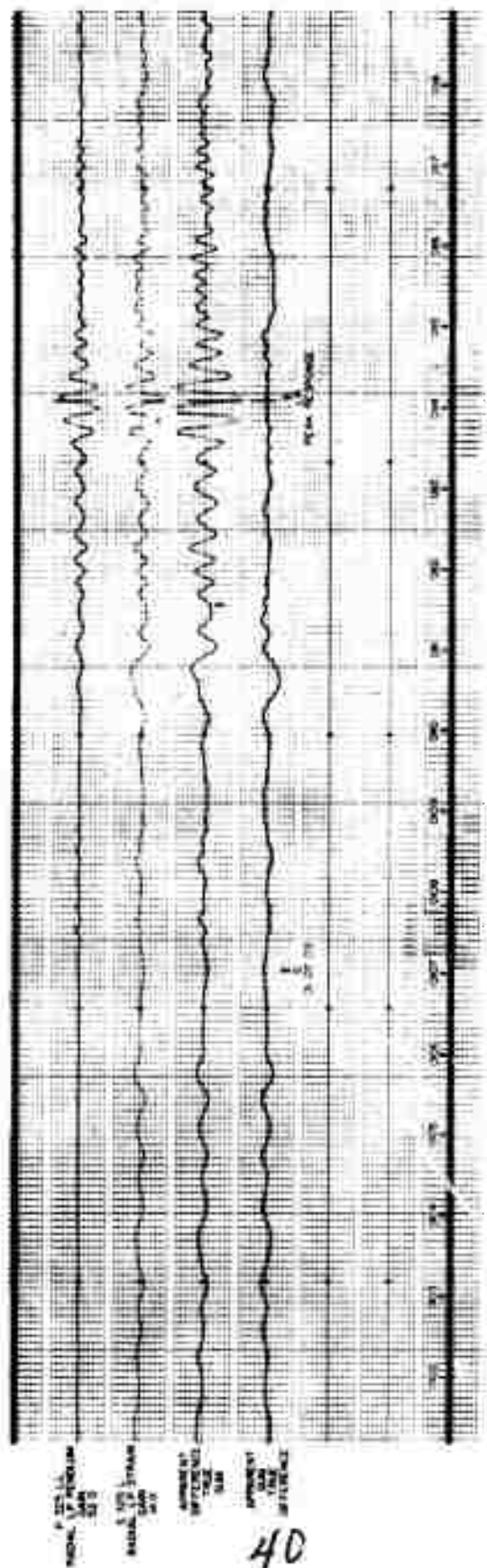Figure 22. Analog computer analysis Chiapas earthquake 19 May 1970.

39

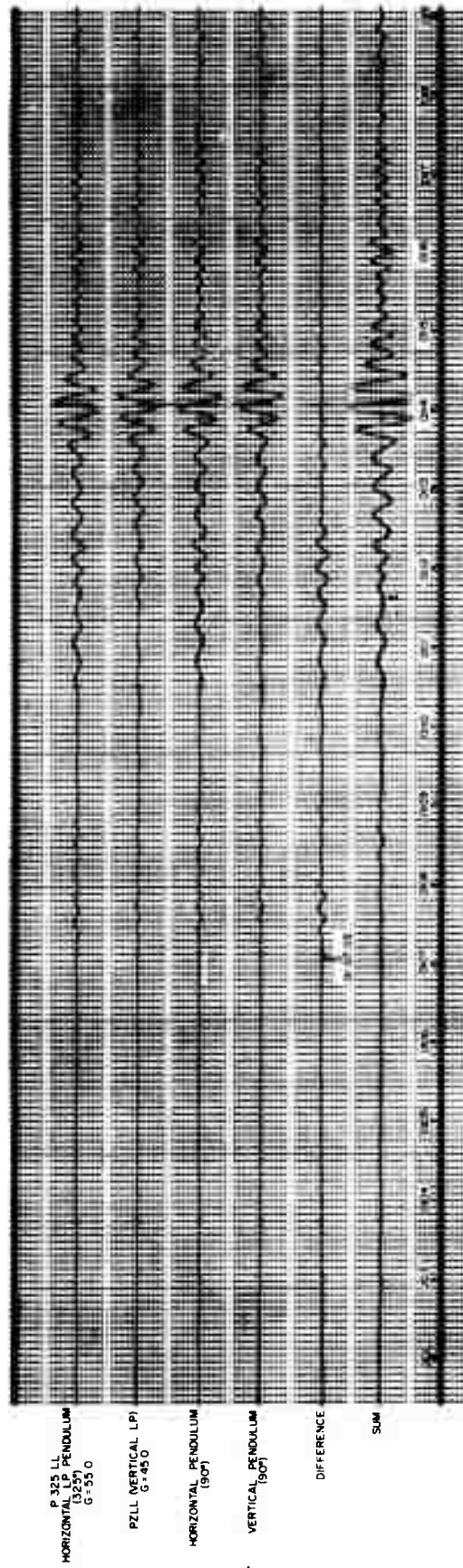Figure 23. Analog computer analysis Chiapas earthquake 19 May 1970.

40

Figure 24.   Analog computer analysis Chiapas earthquake
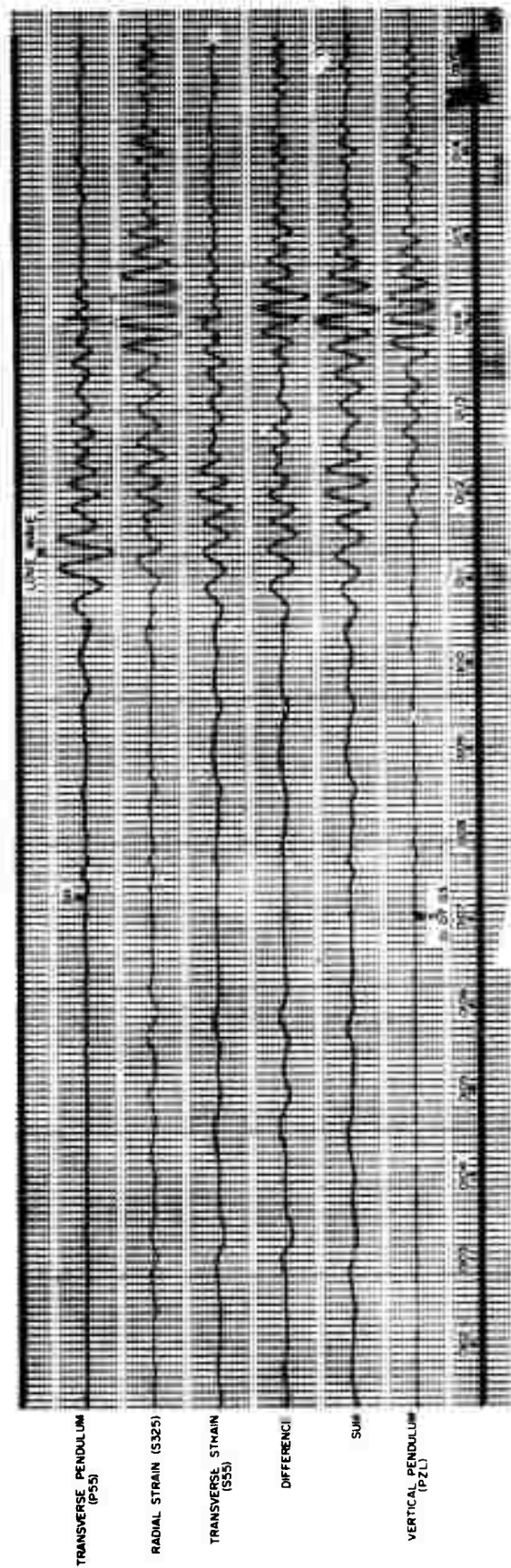19 May 1970.

41

Figure 25. Analog computer analysis Chiapas earthquake 19 May 1970.

42

APPENDIX I
DATA FROM USC&GS PDE CARDS

43

Data From USC&GS PDE cards

		ORIGIN				QCAZ
24708	5/19/70	00 57 11.8	14.5N	93.2W	m_b=4.6	Δ = 25.1°
		(Near Coast of Chiapas, Mexico)				Azi = 133.1
24709	5/19/70	02 07 41.5	79.2N	2.5E	m_b=4.8	Δ = 61.9°
		(Greenland Sea)				Azi = 11.3
	5/19/70	02 31 53.7	15.7S	177.1E	m_b=4.3	Δ = 95.7°
		(Fiji Islands)				Azi = 288.2
24719	5/21/70	15 32 54.4	16.8S	167.7E	m_b=4.8	Δ = 91.5°
		(New Hebrides Islands)				Azi = 251.2
	5/21/70	15 46 28.2	14.4N	92.8W	m_b=4.6	Δ = 25.4°
		(Near Coast of Chiapas, Mexico)				Azi = 133.5
23749	5/22/70	14 08 59.9	3.4N	82.8W	m_b=4.8	Δ = 40.5°
		(South of Panama)				Azi = 132.9
24751	5/25/70	16 47 36.0	29.4S	177.8W	m_b=5.5	Δ = 88.2°
		(Kermadec Islands)				Azi = 232.8

44

APPENDIX II

HOMOGENEOUS HALF-SPACE AMPLITUDE AND PHASE ANALYSIS

45

Using the formulation of Ewing et al. (1957) it is possible to derive theoretical formulations for the amplitude and phase relation for the vertical and horizontal strain and pendulum seismographs at a free surface. This development is limited to P and SV waves.

In order to make the results somewhat more general the assumption that $\lambda = \mu$ has not been made (λ and μ are Lamé constants). The results of Gupta (1966) are a special case of results here obtained, since he assumed $\lambda = \mu$. Gupta's analysis did not include the results for the horizontal strain and pendulum.

Figures II-1 and II-2 show the geometry for incident P and SV waves at the free surface of an elastic solid. Using the notation u_x and u_z for horizontal and vertical displacement respectively, and defining

$$r^2 = \tan^2 e = \frac{c^2}{\alpha^2} - 1$$

$$s^2 = \tan^2 f = \frac{c^2}{\beta^2} - 1$$

one obtains the following formulation for vertical displacement at the free surface ($u_z|_o$), vertical strain at the free surface $\partial u/\partial z|_{z=o}$, horizontal displacement at the free surface $u_x|_o$, and the horizontal strain $\partial u_x/\partial x|_o$. The algebra required becomes rather involved and is not included. Additional notation is
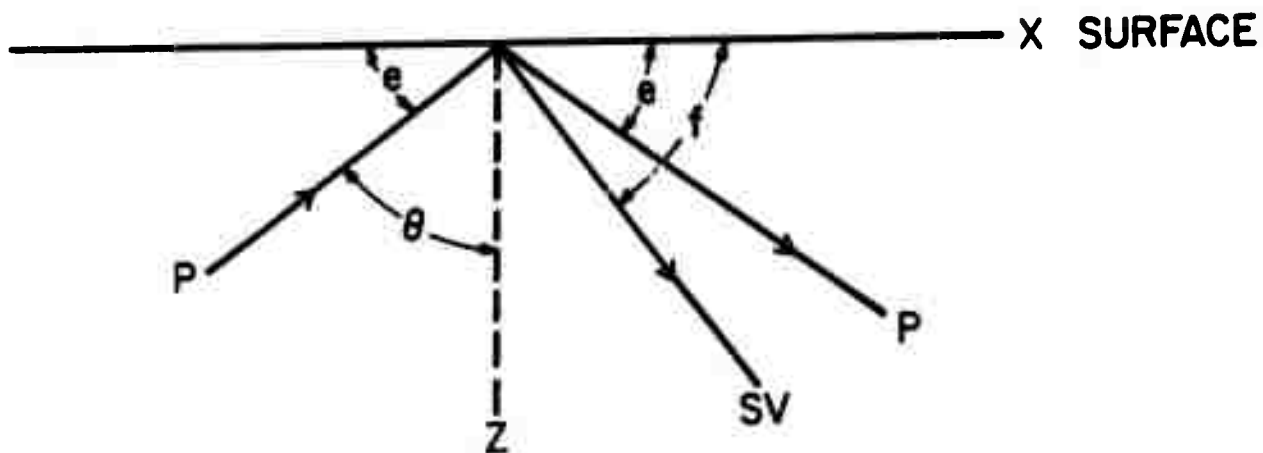
46

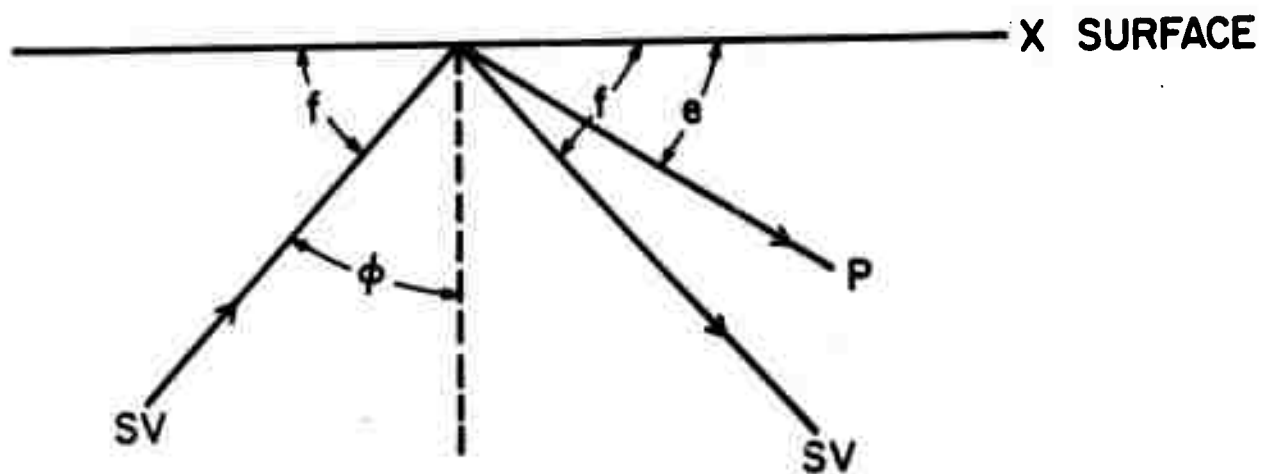Figure II-1. Reflection of P-wave at free surface of an elastic solid.

Figure II-2. Reflection of SV-wave at free surface of an elastic solid.

identical to that of Ewing et al. (1957)

For P-waves:

$$u_z|_o = jkA_1 \; \frac{2r^2(s^2 + 1)\,[\lambda(1 + r^2) + 2\mu\,r^2]}{4\mu\,rs + (s^2 - 1)\,[\lambda(1 + r^2) + 2\mu r^2]}$$

$$\frac{\partial u_z}{\partial z}\bigg|_{z=o} = k^2A_1 \; \frac{4rs\lambda(1 + r^2)}{4\mu rs + (s^2 - 1)\,[\lambda(1 + r^{-2}) + 2\mu r^2]}$$

$$u_x|_{z=o} = - jkA_1 \; 4rs \; \frac{(\lambda + 2\mu)(1 + r^2)}{4\mu rs + (s^2-1)\,[\lambda(1 + r^2) + 2\mu r^2]}$$

$$\frac{\partial u_x}{\partial x}\bigg|_{z=o} = - k^2A_1 \; 4rs \; \frac{(\lambda + 2\mu)(1 + r^2)}{4\mu rs + (s^2 - 1)\,[\lambda(1 + r^2) + 2\mu r^2]}$$

For SV-waves:

$$u_z|_{z=o} = - jkB_1 \; \frac{4\mu rs(s^2 + 1)}{4\mu rs + (s^2-1)\,[\lambda(1 + r^2) + 2\mu r^2]}$$

$$\frac{\partial u_z}{\partial z}\bigg|_{z=o} = k^2B_1 \; s(s^2 - 1) \; \frac{2\lambda(1 + r^2)}{4\mu rs + (s^2 - 1)\,[\lambda(1 + r^2) + 2\mu r^2]}$$

49

$$u_x\Big|_{z=0} = -\,2kjB_1\,\frac{s(s^2-1)\,(\lambda+2\mu)\,(1+r^2)}{4\mu rs + (s^2-1)\,[\lambda(1+r^2)+2\mu r^2]}$$

$$\frac{\partial u_x}{\partial x}\Big|_{z=0} = -\,2k^2B_1\,s(s^2-1)\,\frac{(\lambda+2\mu)\,(1+p^2)}{4\mu rs + (s^2-1)\,[(1+r^2)+2\mu r^2]}$$

The time varying factor exp $[jk(ct - x)]$ has been dropped in each case. Using the above formulae and letting θ be the incident angle for P waves (Figure II-1) one obtains, after some algebraic manipulation:

$$\frac{u_z}{u_x}\Big|_{z=0} = -\,\frac{\cos\theta}{\sin^2\theta}\,\frac{(\lambda+2\mu\cos^2\theta)}{2\mu\left[\dfrac{\lambda+2\mu}{\mu}-\sin^2\theta\right]^{1/2}}$$

$$\frac{\dfrac{\partial u_z}{\partial z}}{u_z}\Big|_{z=0} = -\,\frac{2jk\lambda\mu\sin\theta\left[\dfrac{\lambda+2\mu}{\mu}-\sin^2\theta\right]^{1/2}}{(\lambda+2\mu)(\lambda+2\mu\cos 2\theta)}$$

49

$$\left.\frac{\frac{\partial u_z}{\partial z}}{u_x}\right|_{z=o} \quad z \; jk \; \frac{\lambda}{\lambda + 2\mu}$$

$$\left.\frac{\frac{\partial u_x}{\partial x}}{u_x}\right|_{z=o} = jk \; \frac{\lambda}{\lambda + 2\mu}$$

Similarly for SV waves, where θ is angle of incidence (Figure II-2):

$$\left.\frac{u_z}{u_x}\right|_{z=o} = \frac{2\sin\phi \; [\frac{\mu}{\lambda + 2\mu} - \sin^2\phi]^{1/2}}{\sin 2\phi}$$

$$\left.\frac{\frac{\partial u_z}{\partial z}}{u_z}\right|_{z=o} = \frac{jk\lambda}{2(\lambda + 2\mu)} \; \frac{\cos 2\phi}{\sin\phi \; [\frac{\mu}{\lambda + 2\mu} - \sin^2\phi]^{1/2}}$$

$$\left.\frac{\frac{\partial u_z}{\partial z}}{u_x}\right|_{z=o} = jk \; \frac{\lambda}{\lambda + 2\mu} \quad 50$$